UNIVERSITY of SCIENCE and TECHNOLOGY

POLITEHNICA BUCHAREST

DOCTORAL SCHOOL of ELECTRICAL ENGINEERING

EXTENDED ABSTRACT
Ph. D. THESIS

Contributions on the reuse of electric vehicle batteries

Ph. D. Student:

Ing. Violeta Georgiana DELIU (DOGARU)

Ph. D. Supervisor:

Prof.Univ.Dr.-Ing.Habil. Valentin NĂVRĂPESCU

BUCHAREST
2025

Content

1. Introduction 5
Presentation of the doctoral thesis domain 6
1.1. Scope of the doctoral thesis 6
1.2. Content of the doctoral thesis 7
2. Batteries used in automotive applications 8
2.1. General concepts 8
2.2. Types of batteries used in electric vehicles 8
2.3. Battery life of electric vehicles. Replacement thresholds 9
2.4. Conclusions 9
3. Potential value of second-life batteries 10
3.1. Electric Vehicle Battery Recycling 10
3.2. Reuse of electric vehicle batteries 10
3.3. Conclusions 10
4. Photovoltaic systems 11
4.1. Types of photovoltaic systems 11
4.2. Improving photovoltaic systems 11
4.3. Development of on-grid photovoltaic systems on the residential and commercial market in Romania 11
4.4. Evolution of the number of prosumers in Romania 12
4.5. On-grid photovoltaic systems – a challenge for the national low voltage grid 12
5. Presentation of the current photovoltaic system 13
5.1. General technical characteristics 13
5.2. Wiring diagram of the existing system 14
6. Presentation of second-life battery used 16
6.1. General technical characteristics 16
6.2. Analysis of the purchase process of a pack of 19 modules of the Hyundai Kona Electric 64 kWh battery 17
7. Extending and optimizing the PV system: integrating an AC-coupled configuration 19
7.1. Newly added components and their role 19
7.2. Principiul de funcționare al configurației AC-coupled 20
7.3. Choosing the BMS and optimizing the LG Chem 15s3p battery pack 23
7.3.1. BMS Identification 23

7.3.2. Determination of the optimal loading/unloading parameters and analysis of the obtained data 24
8. Determining the degree of wear of the second-life battery before and after integration into the photovoltaic system 26
8.1. General principles for evaluating the electrical performance of the second-life battery 26
8.2. Presentation of laboratory equipment "Battery testing" 26
8.3. Static Capacity Test 27
8.3.1. Static capacity test when purchasing cells 28
8.3.2. Static capacity test after use in PV system 31
8.3.3. Analysis and conclusions 33
8.4. Hybrid Pulse Power Characterization Test - HPPC 34
8.4.1. HPPC Test When Purchasing Cells 35
8.4.2. HPPC test after use in PV system 37
8.4.3. Analysis and conclusions 39
8.5. Test for determining internal impedance - EIS 41
8.5.1. EIS test when purchasing cells 41
8.5.2. EIS test after cell use in the photovoltaic system 43
8.5.3. Analysis and conclusions 44
9. Alternative modeling and simulation of hybrid operation of residential PV system 45
9.1. Objective of the simulation 45
9.2. Modeled System Configuration 45
9.3. Modeling and simulation of the hybrid system in Matlab/ Simulink 46
9.4. Interpretation of simulation results 47
9.5. Conclusions 48
10. Comparative analysis of PV system performance with and without energy storage: energy and economic impact 49
10.1. Energetic impact 49
10.1.1. Energy analysis of the photovoltaic system in on-grid configuration (basic configuration) 49
10.1.2. Energy analysis of the photovoltaic system in hybrid configuration (with the integration of energy storage) 50
10.1.3. Comparative analysis 51
10.2. Economic impact 53
10.2.1. Economic analysis of the photovoltaic system in on-grid configuration (basic configuration) 53

10.2.2. Economic analysis of the photovoltaic system in hybrid configuration (with the integration of energy storage) 54
10.3. Amortization of the investment 55
10.3.1. Return on investment for on-grid photovoltaic system 55
10.3.2. Amortization of the investment for the hybridized PV system 55
10.4. Conclusions 56
11. Conclusions 57
11.1. Results obtained 58
11.2. Original contribution 60
11.3. Prospects for further development 61

Chapter 1

Introduction

The accelerated growth of the electric vehicle market is one of the most visible technological changes of the last decade, driven by advances in battery technology, regulations to limit greenhouse gas emissions and reduce production costs. However, this trend has the side effect of accumulating an increasing volume of end-of-life batteries in e-mobility applications. In general, after a period of approximately 6 to 8 years of operation, batteries used to power vehicles no longer meet the strict requirements for energy density, discharge power and range, and are considered unsuitable for automotive applications, even if they retain a significant functional capacity.

In this context, end-of-life batteries, conventionally referred to as "second-life", represent a category of electrochemical resources that, although they no longer meet the original performance specifications, can be reintroduced into the economic circuit by reconfiguration and reuse in less demanding stationary applications. In particular, when their capacity falls below the threshold of 70 – 80% of the initial nominal value, the performance no longer corresponds to the standards imposed by electric traction applications, but can be used efficiently in stationary applications, where energy density and power requirements are considerably lower, thus contributing to waste reduction, increasing resource efficiency and supporting sustainable energy systems.

Recycling these batteries currently remains a difficult, complex and expensive operation. In addition, globally, the current recycling capacity is insufficient to process the expected volumes. This context creates the premises for the development of alternative strategies, and the possibilities for capitalizing on *second-life* batteries are diverse, including back-up systems for critical infrastructures, industrial equipment, telecommunications networks and, with increasing relevance, renewable energy storage units. In the latter field, the integration of batteries into photovoltaic systems has significant advantages: storage of surplus energy produced during periods of high irradiance, its availability at times of high consumption or low production and increased self-consumption.

In parallel, the adoption of photovoltaic systems is experiencing accelerated growth, both in residential and commercial environments. On-grid photovoltaic systems, which currently constitute the most widespread residential configuration, are characterized by direct connection to the electricity grid. Although this architecture allows the sale of surplus energy to the operator, the massive increase in the number of such systems can lead to undesirable effects on the grid: local overvoltages, frequency variations and restrictions imposed by operators during periods of overproduction. Under these conditions, the integration of *second-life* batteries in hybrid configurations (on-grid + storage) is not only a solution for optimizing local consumption, but also a means of reducing the negative impact on the electricity grid.

Presentation of the doctoral thesis domain

This doctoral thesis provides an in-depth examination of a contemporary topic situated at the intersection of two strategic research areas: the transition towards renewable energy sources and the sustainable reuse of technologies originating from the electric vehicle industry. Specifically, the study investigates the integration of second-life batteries recovered from electric vehicles into an on-grid photovoltaic system, proposing an applied model together with a detailed assessment of performance under real operating conditions.

Through its applicative and interdisciplinary approach, the thesis makes a relevant contribution to the development of knowledge on the extension of the life cycle of batteries, the efficient integration of renewable sources in electricity grids and the strengthening of sustainability in the energy field.

This paper aims not only to demonstrate practical integration, but also to contribute to understanding the role that second-life batteries can play in the sustainable energy transition, especially in the context of an increasingly renewable, prosumer electricity grid.

1.1. Scope of the doctoral thesis

The aim of this study is to evaluate the potential for reuse of *second-life* batteries from electric vehicles in current applications such as energy storage units for residential photovoltaic systems. The integration of these batteries is analyzed in the context of the problems associated with the operation of on-grid photovoltaic systems on the power grid, such as the occurrence of local surges, restrictions on energy injection and the loss of part of the photovoltaic production during periods of low consumption.

The solution investigated consists of hybridizing existing photovoltaic systems by adding a storage unit made of *second-life* batteries, configured to ensure electrical and functional compatibility with the equipment already installed. This approach aims to increase self-consumption, reduce dependence on the public grid and make efficient use of locally produced energy.

The analysis aims to investigate the effects of battery integration on the energy and economic indicators of the system, with a focus on energy independence, overall efficiency and return on investment. In parallel, the electrochemical behavior of batteries in stationary applications is evaluated, taking into account the practical advantages and limitations of the proposed solution.

Against the backdrop of the energy transition to renewable sources, which requires efficient methods of balancing electricity grids, and the continuous increase in the volume of end-of-life batteries from electric vehicles, this research aims to:

- investigate the technical characteristics, performance and wear of second-life batteries over an extended life cycle;
- demonstrate the technical and economic feasibility of integrating them into a functional AC-coupled photovoltaic system;
- provide a solid scientific basis for the use of second-life batteries in stationary energy storage applications at residential or commercial level.

1.2. Content of the doctoral thesis

This paper analyzes the practical integration of a pack of second-life batteries from an electric vehicle (Hyundai Kona Electric 64 kWh) into an existing on-grid photovoltaic system, aiming to assess the technical feasibility, performance, wear and tear impact. In the first part, the technological foundations of batteries used in automotive applications are presented, followed by an analysis of the potential of second-life batteries, including difficulties, industrial initiatives and research projects.

Subsequently, the types of photovoltaic systems are detailed, with a focus on the evolution of on-grid systems in Romania, highlighting the development opportunities and the current limits of the low voltage network. In the following chapters, the details of the photovoltaic system used as the test platform are presented, as well as the characteristics of the selected second-life battery pack from a Hyundai Kona Electric vehicle.

The applicative part of the work aims to configure an AC-coupled solution for the integration of the second-life battery, followed by a detailed experimental evaluation of its degree of wear – before and after integration – through standardized tests: static capacity test, characterization of the power of hybrid pulses and electrochemical impedance spectroscopy.

Below is described a process of modeling and simulation of the hybrid operation of the photovoltaic system, proposed as an alternative to conventional hybridization solutions. Thus, the feasibility of extending an existing residential photovoltaic system by integrating a secondary energy source, in the form of a battery, into a DC-coupled architecture, without the need to modify the already installed on-grid inverter is highlighted.

The following chapter presents a comparative assessment of the performance of the photovoltaic system in the initial configuration and after the integration of an energy storage system, thus demonstrating, based on the data obtained, the advantages, limitations and technical-economic potential of hybridization by implementing a local storage solution.

The conclusions chapter summarizes the main results and contributions of the research, highlighting how the set objectives were achieved and the impact of the proposed solutions on the field studied. In the first part, the results obtained are presented, with emphasis on their relevance in relation to the issues addressed and on the validation of the hypotheses formulated. Subsequently, the author's original contributions are presented, emphasizing the elements of methodological, technical and applicative novelty.

A separate section is dedicated to listing the papers published within and in connection with the research theme, reflecting the dissemination of the results to the scientific community. Finally, the future directions of development are discussed, taking into account both the deepening of the investigated aspects and the extension of the applicability of the proposed solutions in practical contexts and evolving technological scenarios.

Chapter 2

Batteries used in automotive applications

2.1. General concepts

Initially used strictly to power the auxiliary electrical systems of conventional internal combustion engine vehicles, batteries have evolved significantly from both a technological and a functional perspective. Under current conditions, they are central elements in the architecture of hybrid and electric vehicles, where they provide the main source of energy for propulsion. The increase in demand for sustainable transport has accelerated innovation, geared towards batteries with high energy density, durability and increased safety. Currently, the choice of storage technologies is influenced by both technical performance and costs, recyclability and environmental impact.

2.2. Types of batteries used in electric vehicles

The diversity of automotive applications has led to the development of advanced types of batteries, capable of meeting the requirements of energy density, durability, safety and economic efficiency. The evolution of electrochemical technologies began with nickel-based batteries, of which Ni-Cd and Ni-MH are still used in current applications, being appreciated for their robustness and extended lifespan, but limited by environmental impact and low energy density [1], [2], [3]. The major advancement has been the introduction of lithium-based batteries, especially Li-ion and Li-polymer, which offer higher energy densities, high performance and minimal maintenance, and are currently the dominant technology in electric vehicles [4]. Various Li-ion chemistries (LCO, LMO, NMC, NCA, LFP, LTO) allow for a varied trade-off between autonomy, safety, cost and lifespan [5], [6], [7], while Li-polymer batteries add the advantage of constructive flexibility. In parallel, Li-air batteries are emerging as a promising solution for the future, due to their potentially higher energy density, but remain in the experimental phase [8]. The integration of these technologies is supported by advanced thermal management systems, which optimize performance and safety under various operating conditions. Thus, the transition from nickel to lithium-based batteries reflects a continuous evolution towards more efficient, safe and sustainable technologies capable of supporting the widespread adoption of electric mobility.

2.3. Battery life of electric vehicles. Replacement thresholds

Electric vehicle batteries are essential components, directly influencing the range, performance and operating costs of an electric vehicle. Research shows that when capacity falls below the threshold of 70–80% of the initial value, reliability decreases significantly, and degradation manifests itself in both reduced capacity and increased internal resistance [9], [10], which limits energy efficiency. Below this threshold, batteries become more sensitive to current and temperature variations, requiring additional charging cycles and losing energy efficiency, which justifies their replacement in automotive applications. Manufacturers' policies confirm this limit through guarantees that set minimum thresholds of 70–75% of the initial capacity and a maximum number of kilometers traveled.

Table 2.1 summarises the battery replacement thresholds set by the main EV manufacturers:

Table 2.1 Electric vehicle battery replacement thresholds

Crt.no.	Manufacturer	EV Model	Guaranteed capacity threshold	Battery warranty
1.	Tesla	S, X, Cybertruck	Under 70% capacity	8years/ 160000km [11]
2.	Nissan	Leaf	Under 75% capacity	8years/ 160000km [12]
3.	BMW	i3, i4, iX	Under 70% capacity	5years/ 200000km [13]
4.	Volkswagen	ID.3, ID.4	Under 70% capacity	8years/ 160000km [14]
5.	Hyundai	Kona Electric	Under 70% capacity	8years/ 160000km [15]
6.	Kia	EV6	Under 70% capacity	7years/ 150000km [16]
7.	Rivian	R1T, R1S	Under 70% capacity	8years/ 200000km [17]

Under these circumstances, the reorientation of degraded batteries to second-life applications, in particular stationary renewable energy storage systems, is a sustainable option, adapted to less demanding requirements than those in the automotive sector.

2.4. Conclusions

The analysis of the types of batteries used in electric vehicles highlights a constantly developing field, influenced by technical, economic and environmental requirements. Currently, lithium-ion batteries are in a dominant position, offering a favorable compromise between energy density, lifespan and integration into vehicle architectures, but are limited by sensitivity to extreme temperatures, chemical degradation processes and raw material costs. Other technologies, such as Ni-MH or experimental Li-air batteries, outline alternative solutions for specific requirements, but do not yet offer universal applicability. The choice of battery type is conditioned by autonomy, operating conditions, costs and charging infrastructure, which leads to solutions based on functional compromises. Future research directions focus on improving safety, extending lifespan and reducing environmental impact, without compromising the functional performance of energy systems integrated into electric vehicles.

Chapter 3

Potential value of second-life batteries

3.1. Electric Vehicle Battery Recycling

The accelerated growth in the number of electric vehicles globally is amplifying the demand for batteries, which requires sustainable solutions to manage them at the end of their useful life. The most efficient options are reuse and recycling, which are considered complementary processes within the circular economy. Recycling focuses on the recovery of valuable metals (cobalt, nickel, lithium) through hydrometallurgical and pyrometallurgical technologies [18], [19], [20], each with advantages and limitations in terms of cost, energy consumption and environmental impact [21]. Thus, reuse followed by recycling emerges as an optimal strategy for extending the life cycle of batteries and reducing environmental impact.

3.2. Reuse of electric vehicle batteries

After the capacity drops below the optimal threshold for electric vehicle performance, batteries become inefficient for mobility, but remain suitable for stationary uses, back-up systems or grid balancing applications. Due to their high energy density and superior cyclability, NMC, LFP and NCA technologies are the most commonly used. However, integration into *second-life* applications poses challenges related to electrochemical degradation, variations between modules and safety requirements [22], but these can be addressed through advanced battery management systems and precise health assessment (SOH) methods [23], [24]. Thus, second-life batteries are emerging as viable and sustainable solutions for storing renewable energy and increasing the flexibility of electricity grids [25], [26].

3.3. Conclusions

When possible, reusing the entire battery without dismantling is the preferred solution; otherwise, modules and cells can be tested and reconfigured into new packages. The collection, sorting and testing process is essential, but it raises technical and safety challenges, amplified by the constructive diversity of existing packages on the market.

This general framework highlights the potential of second-life applications and paves the way for specific case studies, in which reused batteries are integrated into systems such as photovoltaics, local power grids or customised stationary applications.

Chapter 4

Photovoltaic systems

4.1. Types of photovoltaic systems

The most widely used types of solar cells are those made of monocrystalline and polycrystalline silicon, due to the balance between efficiency, cost and durability. They are found in a variety of photovoltaic systems, adapted to various applications and operating conditions.

Residential and commercial systems are designed to meet the energy needs of homes and large buildings, either by connecting to the grid (on-grid) or through autonomous solutions (off-grid). In isolated areas, hybrid or autonomous systems are used, and to increase efficiency, some installations use sun tracking mechanisms or are implemented in floating form, on aquatic surfaces. On a large scale, photovoltaic parks cover large areas and are directly connected to electricity grids, while portable and infrastructure-integrated systems offer flexible solutions for mobile applications or for reducing the carbon footprint in urban projects. The choice of an optimal configuration depends on the technical and economic context and the energy objectives pursued, each category having both advantages and specific limitations.

4.2. Improving photovoltaic systems

The improvement of photovoltaic systems is an area of continuous research and development, with a focus on optimizing performance, reducing costs and expanding integration possibilities. Among the major innovations are: the evolution of photovoltaic cells, thin-film technologies that offer extensive applicability or tandem cells, capable of achieving higher yields by using multiple absorption layers.

Another key area is the development of inverters [27], where recent advances include the integration of artificial intelligence and fuzzy control for conversion optimization and reactive power management [28], [29]. Innovations in inverter technology, as well as the adoption of microinverters and autonomous microgrid systems [30], contribute to reducing harmonic distortions, increasing stability and expanding the use of photovoltaic energy in areas without energy infrastructure.

4.3. Development of on-grid photovoltaic systems on the residential and commercial market in Romania

In the context of the current energy transition, marked by the need to reduce dependence on fossil resources and promote renewable sources, on-grid photovoltaic systems have emerged as the predominant solution. Their choice is supported by several factors: financial stability

conferred by predictable energy production independent of market volatility; government and international support through incentive policies and tax incentives; the possibility of capitalizing on the surplus energy injected into the grid, with a positive impact on the amortization of the investment; relatively easy integration into existing infrastructure; reducing carbon emissions and contributing to environmental protection; as well as the community-wide benefits of creating a distributed source of energy. However, the adoption of these systems depends on the specific requirements of users and the local specificities of the electricity grid.

4.4. Evolution of the number of prosumers in Romania

The concept of prosumer, resulting from the association of the terms 'producer' and 'consumer', designates an entity capable of producing, consuming, storing and trading energy from renewable sources [31]. In Romania, the first prosumer was connected to the national grid in 2012 [32], and further development was supported by legislative adaptations and financing programs such as *Casa Verde Fotovoltaice* and *Electric UP.* The evolution of the regulatory framework, correlated with the European objectives set out in Directive (EU) 2018/2001 (RED II) [33], has led to an accelerated increase in the number of prosumers and installed power, especially after 2020. The data reported by ANRE indicate a rapid expansion of this community, from a few hundred prosumers at the beginning of 2020 to over 40000 at the end of 2022 [34], thus strengthening the transition to a decentralized energy model. In the absence of large-scale deployed storage solutions, the trend remains focused on capitalizing on solar photovoltaic energy, with prospects for continued growth with the implementation of support programs in the coming years.

4.5. On-grid photovoltaic systems – a challenge for the national low voltage grid

The deployment of photovoltaic systems generates considerable benefits [35], but with increasing integration, technical challenges arise that influence both the quality of energy and the safety of distribution networks. These include the occurrence of reverse flow of power, voltage fluctuations caused by the intermittent nature of solar production, phase imbalances in single-phase inverters, and harmonic distortions induced by power electronics. These phenomena can lead to overloads, non-compliance with power quality standards [36] and malfunction of protective equipment.

Possible solutions include modernizing the infrastructure by integrating storage systems, implementing advanced monitoring and control technologies, adopting high-performance equipment, and complying with energy quality regulations. Overall, the transition to a high degree of PV system integration requires a balanced approach between the sustainability benefits and the associated technical challenges.

Chapter 5

Presentation of the current photovoltaic system

5.1. General technical characteristics

The analyzed photovoltaic system is configured as an on-grid system, connected to the electricity grid and dependent on it for the management of the energy flow. It is composed of photovoltaic panels, an on-grid inverter, a monitoring system and adequate protections for the safety and optimal operation of the equipment.

The electricity generation is carried out by an assembly of 12 Sharp NU-JD540W photovoltaic panels. With the help of the *Solar.creator* application [37] made available to Fronius users, they were organized into two strings, one consisting of 9 modules and the other of 3 modules (Figure 5.1). The panels are connected to the DC panel using 4 mm² conductors, the size chosen to keep the same section according to the manufacturer's specification, and their frames are connected to the ground socket.

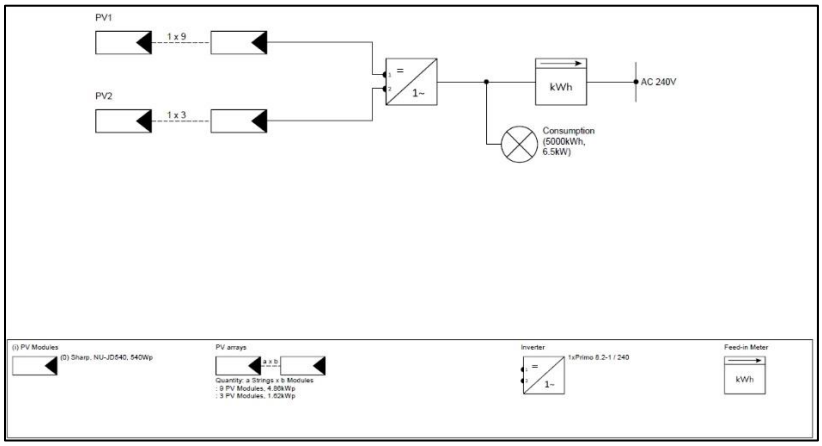


Figure 5.1 Photovoltaic panel connection diagram according to the specialized website

The photovoltaic system has been sized to ensure optimal compatibility with the Fronius Primo 8.2-1 single-phase inverter, with a nominal power of 8.2 kW and a maximum efficiency of 98.1%. The configuration includes two strings: one consisting of 9 Sharp NU-JD540W panels (Vmpp = 374.76V, Impp = 12.97A, Voc = 453.06V) and a second of 3 panels (Vmpp = 124.92V, Impp = 12.97A, Voc = 151.02V), totaling 6.48kWp. The parameters of the strings fall within the working range of the two MPPT trackers of the inverter (80 – 800V, max. 1000V DC), optimized by Dynamic Peak Manager technology. The configuration is completed by 6 spare panels for expansion or replacement. Energy flow monitoring is carried out with the Fronius Smart Meter TS 100A-1, a bidirectional meter connected via Modbus RTU/RS485 to the inverter and to the Fronius Datamanager 2.0 system. It ensures real-time data transmission and analysis through the Solar.web platform, with WLAN, Ethernet and USB connectivity.

5.2. Wiring diagram of the existing system

The nomenclature page (Figure 5.2) in the wiring diagram provides a detailed list of components used in the PV system, including protective devices, connection cables, fuses, and main equipment. This section helps you understand your system configuration and diagnose or maintain it.

Among the main components found in the nomenclature are:

- AC (Figure 5.3) and DC (Figure 5.4) electrical panel, which distributes power and provides circuit protection;
- Fronius Primo 8.2-1 inverter;
- Fronius Smart Meter TS 100A-1, used for energy flow monitoring;
- Surge protection device for the protection of equipment against voltage fluctuations;
- differential and automatic fuses, which prevent overloads and short circuits;
- connection cables, with precise specifications for DC and AC.

Elemente electrice

Nr. Crt.	Descriere	Cod schema	Cantitate (buc/ metri)
1	FDCP -> Firida de distribuție, contorizare și protecție	SE-4 RED 0.4 kV	N/A
2	Bară de egalizare potențial pentru exterior	PEN	1
3	Bloc masura si protectie monofazat	BMPM 50A	1
4	Contor electric dublu sens	C 01	1
5	Siguranta cu protectie diferentiala 50A	ID 50A	1
6	Cablu alimentare tablou AC	Cablu CYABY	1
7	Tablou electric AC	Tablou AC	1
8	Contor inteligent Fronius TS 100A-1	C 02	1
9	Descarcator supratensiune 275V AC	D AC1	1
10	Siguranta cu protectie diferentiala 40A	F 0 40A	1
11	Siguranta priza 16A	F 1 16A	1
12	Siguranta priza 16A	F 2 16A	1
13	Siguranta lumina 10A	F 3 10A	1
14	Siguranta lumina 10A	F 4 10A	1
15	Siguranta cu protectie diferentiala 40A	F 5 40A	1
16	Cablu alimentare Invertor Fronius	Cablu1 CYABY	1
17	Invertor Fronius 8.2-1 monofazat	I01	1
18	Conductor monofilar DC rosu 4mmp	N/A	1
19	Conductor monofilar DC negru 4mmp	N/A	1
20	Serie 9 panouri X 540W Sharp NU-JD540W	String 1	1
21	Serie 3 panouri X 540W Sharp NU-JD540W	String 2	1
22	Soclu conductor + fuzibil 20A	F1 01	1
23	Soclu conductor + fuzibil 20A	F1 02	1
24	Tablou electric DC	Tablou DC	1
25	Separator 0-1	Q1 01	1
26	Separator 0-1	Q1 02	1
27	Separator bipolar + 2Xfuzibil 15A	F2 01	1
28	Separator bipolar + 2Xfuzibil 15A	F2 02	1
29	Descarcator supratensiune 500V DC	D DC1	1
30	Descarcator supratensiune 500V DC	D DC2	1

Figure 5.2 Nomenclature of electrical elements



Figure 5.3 AC Electrical Panel



Figure 5.4 Fronius Primo 8.2-1 DC panel and inverter

The electrical system is organized into two main circuits: the direct current (DC) circuit and the alternating current (AC) circuit. They ensure the flow of energy from the solar panels to the final consumers and the electricity grid. The DC circuit (Figure 5.5) is composed of two strings of photovoltaic panels, connected to the DC panel by 4mm² conductors. It includes 500V DC surge arresters, installed to protect equipment from sudden voltage swings. The energy generated by the panels is transmitted to the Fronius Primo 8.2-1 inverter, where the conversion to AC current takes place.

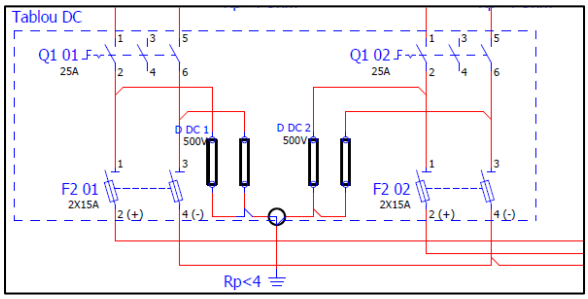


Figure 5.5 The electrical components in the DC panel

The AC circuit includes the inverter, the AC panel (Figure 5.6), and the monitoring system. The Fronius Primo 8.2-1 inverter, together with the "*F 5*" protection element, converts direct current into alternating current and manages the energy flow to consumers and the electricity grid. The power is distributed through the AC panel equipped with differential fuses and 275V AC surge protection.

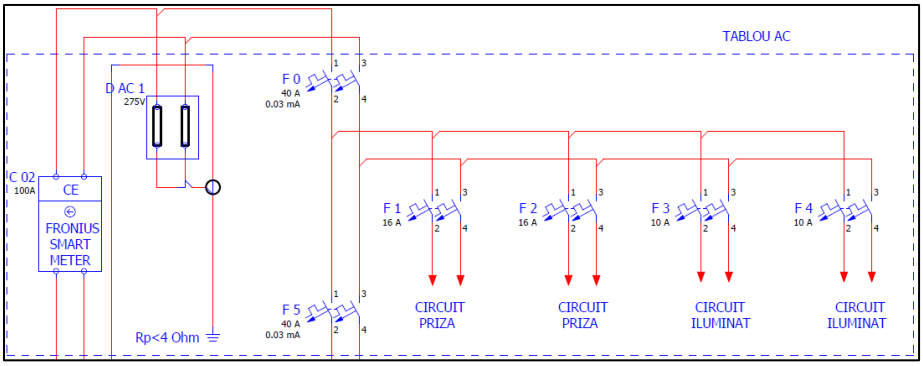


Figure 5.6 Electrical components in the AC panel

The Fronius Smart Meter TS 100A-1 monitors consumption and energy injected into the grid, optimizing energy resource management via the Fronius Solar platform.

Chapter 6

Presentation of second-life battery used

6.1. General technical characteristics

The battery installed on the Hyundai Kona Electric (2019–2021) is an essential element of the vehicle's architecture, being optimized for energy density and high operational performance. With a nominal capacity of 64 kWh, it ensures a WLTP-certified range of up to 449 km, positioning the model as a notable competitor in the electric vehicle segment.

The battery is Li-ion and uses cells manufactured by LG Chem, arranged in a modular configuration of 98s3p. The modular structure offers the possibility of adapting and increasing the capacity of the system according to the requirements of the application, while facilitating maintenance operations and reducing the complexity of interventions. It is organized in a complex modular structure, composed of two types of packs (Figure 6.1):

- three packs of 20 modules each: these provide a nominal voltage of 72V each (20 × 3,6V).
- two packs of 19 modules each: these provide a nominal voltage of 68.4V each (19 × 3,6V).

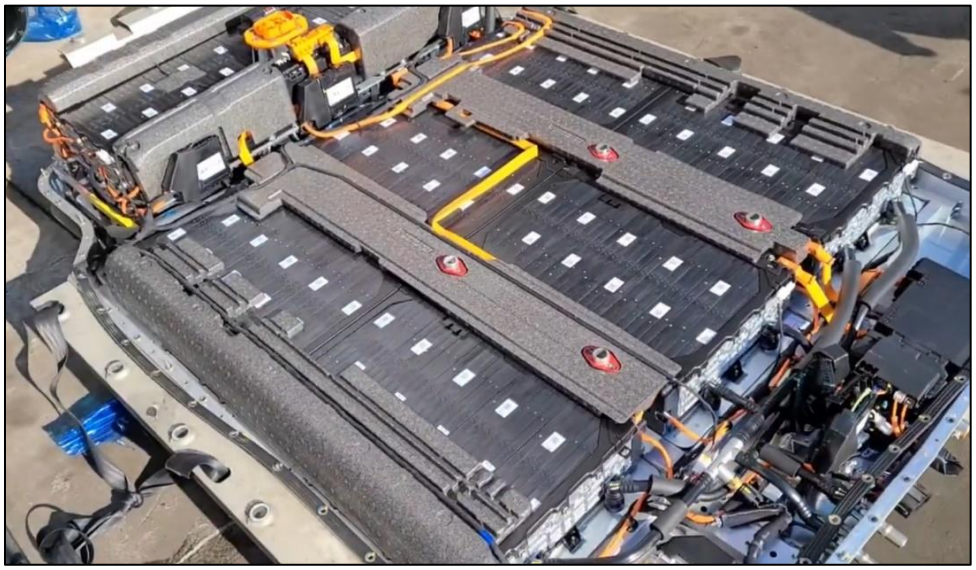


Figure 6.1 Hyundai Kona 64 kwh battery overview

The five packs are connected in series to achieve the total battery voltage rating of approximately 352.8V. This modular organization allows optimal use of space in the vehicle chassis and simplifies maintenance or replacement of defective components. The integration of the packages is done in a compact assembly, designed to optimize heat dissipation and ensure mechanical safety. The BMS monitors the operational parameters of each component,

including voltage, current, and temperature, preventing imbalances and maximizing the durability of charge-discharge cycles.

6.2. Analysis of the purchase process of a pack of 19 modules of the Hyundai Kona Electric 64 kWh battery

As part of this study, a package of 19 modules, an integral part of the original Hyundai Kona Electric 64kWh battery, was purchased from a supplier of reusable components for electric vehicles. The choice of this assembly was aimed at integrating into energy storage applications the detailed assessment of the condition of the cells, taking into account the wear accumulated during the previous operation of the vehicle.

Each module, consisting of three Li-ion cells connected in parallel, has a nominal capacity of 175.2Ah (58.4Ah x 3), respecting the original 98s3p battery architecture (Figure 6.2).



Figure 6.2 Lg Chem cell

All components used in the assembly of the battery pack (Figure 6.3) are marked with standardized markings indicating the year of manufacture 2019. These markings contain information about the production batch, the production line and the exact date of manufacture of each component. This finding is consistent with the initial use of the battery in a Hyundai Kona Electric vehicle produced between 2019 and 2021.



Figure 6.3 View of 19 modules pack

Markings are present both on individual modules and on the mechanical and electrical elements of the package, including wiring and insulating materials. Analysis of these markings highlighted the uniformity of the components, suggesting that the entire package comes from the same production line, with no subsequent replacements. This is an important feature for evaluating system reliability, as it guarantees that all components have been manufactured and tested to the same standards.

In order to evaluate the electrochemical behavior of the cells in the initial state and after use in the photovoltaic system, it is necessary to select a representative sample from the configured package, consisting of 15 modules (45 cells). The selection of cells is carried out based on a methodology in accordance with the ISO 2859-1 standard – *Sampling procedures for inspection by attributes* [38], witch provides a framework for batch sampling for inspection and testing purposes.

The batch of 45 available cells is organized in the form of 15 individual modules, each containing 3 cells in parallel, conventionally referred to by the letters A, B and C (Figure 6.4).

In order to ensure a representative dispersion and to avoid concentrating the selection in a limited area of the package, a selection strategy was adopted, with a regular interval of 9 cells between successive choices. Thus, the following cells were selected for analysis: 1A, 4B, 7C, 11A, 14B. This choice was aimed at respecting the spacing within the batch and an internal variation of the positions in the modules, selecting in a balanced way cells of type A, B and C.

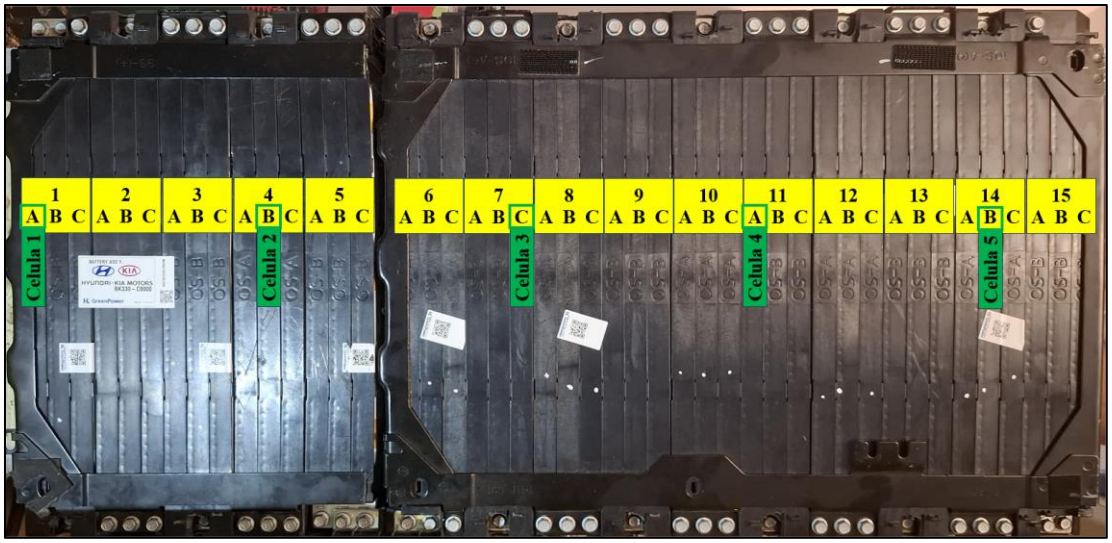


Figure 6.4 The 5 cells selection scheme

Through this selection method, both a uniform distribution of sampling points within the batch and a diversification of the internal positioning of the cells in modules were pursued, in order to reduce the potential influences of the physical position on the experimental results, such as local temperature variations or contact resistances.

The configuration of these 15 modules in series has led to a system with the following characteristics: nominal voltage – 54V, total capacity – 175.2Ah and total available energy – approximately 9.46 kWh. These characteristics make the system suitable for stationary storage applications, providing enough energy to supply electrical loads during periods of high demand or in the absence of photovoltaic generation.

Chapter 7

Extending and optimizing the PV system: integrating an AC-coupled configuration

Modern photovoltaic systems require flexible solutions for the efficient integration and management of the energy produced. The initial configuration, based on the Fronius Primo 8.2.1 inverter, is to be extended by an AC-coupled architecture, which includes additional equipment for the creation of a microgrid. This solution allows optimized consumption management and greater adaptability to variations in energy demand.

By integrating the Fronius Primo inverter on the Multiplus II output, the system becomes a microgrid, managed independently of the main power grid. In this configuration, the energy produced by the panels is injected into the AC circuit managed by the Multiplus II. The consumption is covered by photovoltaic production or, failing that, by a storage system to be selected later. Control equipment allows automatic adjustment of energy distribution, optimizing the use of available resources.

7.1. Newly added components and their role

System performance is enhanced by auxiliary components (Figure 7.1): *Victron MultiPlus-II 48/10000/140-100 10kVA inverter/charger*, *Energy Meter ET112* for measuring energy flows in the grid, *Victron Cerbo GX* for equipment coordination, *Victron Smart Shunt 500A* for battery monitoring, *Victron Lynx Distributor* for safe DC distribution, *GX Touch 50 graphical interface* for monitoring and configuring system parameters, as well as the Li-ion battery managed by the *JK-PB2A16S-20P BMS*. The data obtained is centralized and analyzed through the VRM platform, ensuring control, optimization and predictive maintenance.

An important feature of VRM Portal is remote access to equipment configurations. Users can change parameters of the inverter, charge controller, or other compatible devices without the need for physical intervention on the system.

The VRM Portal interface allows you to view graphs of energy consumption, generation and storage, with users having the option to select time frames for data analysis. The portal also supports integration with external systems and data export for advanced analytics.

Thus, the proposed configuration offers a hybrid microgrid model, safe and flexible, capable of meeting modern energy requirements through the efficient integration of photovoltaic production, smart storage and distribution.



Figure 7.1 Installation of added components for system hybridization

7.2. Principiul de funcționare al configurației AC-coupled

It is based on the integration of an on-grid photovoltaic inverter with a hybrid inverter/charger, using a common link in the alternating current (AC) grid [39]. In this architecture, the on-grid inverter injects the energy produced by the photovoltaic panels into the local AC grid, from where it is taken over and managed by the hybrid inverter, which provides power to consumers and charges the batteries. The control of the energy flow is carried out indirectly, through a mechanism called "frequency shifting", whereby the Victron inverter adjusts the frequency of the local AC network (e.g. from 50Hz to 51–53Hz), causing the Fronius inverter, configured in micro-grid mode, to automatically reduce its output when the batteries are almost fully charged. This interaction allows a dynamic optimization of self-consumption and prevents overproduction. The system thus ensures functional compatibility in both operating modes (on-grid and off-grid) without requiring direct communication between inverters, using exclusively the parameters of the AC network for synchronization and control. Since the Multiplus II does not contain the DC-to-AC energy conversion component on the PV panel side, the on-grid inverter has two roles in this architecture:

– converts energy from photovoltaic (DC) panels into AC energy synchronized with the grid (with that of the electricity distributor or with the grid simulated by Victron in backup/off-grid mode);

– it also contains its own Maximum Power Point Tracking (MPPT) system. In this way, it manages direct current from the panels, optimising solar production independently of Victron.

The integration of the Fronius Primo inverter on the Multiplus II output in AC-coupled mode (Figure 7.2) allows the creation of a microgrid, where energy management is done locally, independent of fluctuations in the power grid, including power outages. In this configuration, the energy generated by the photovoltaic panels is injected into the AC circuit.

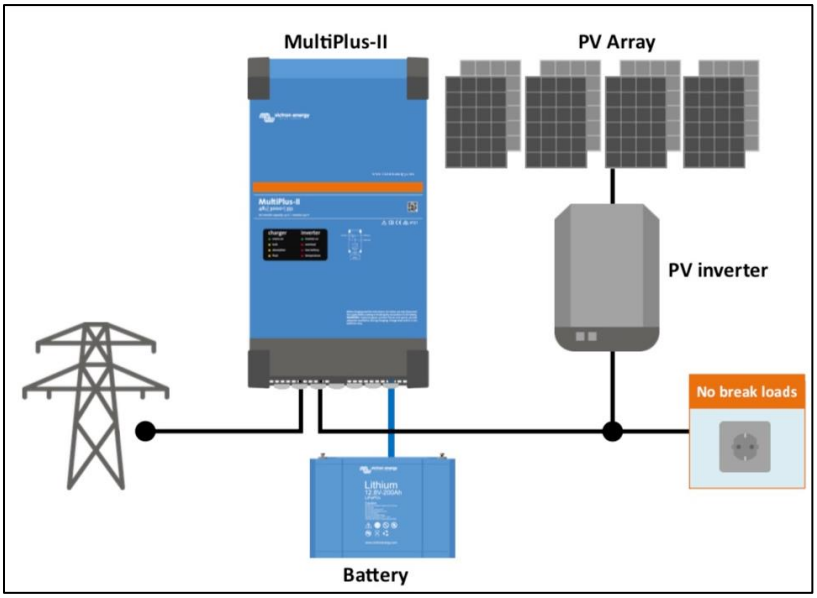


Figure 7.2 AC connection diagram according to [40]

In the wiring diagram of the hybrid PV system, the Multiplus II *I02* inverter is inserted between the mains and the Fronius *I01 inverter*. Compared to the wiring diagram in the on-grid configuration, the elements were separated into two pages: HYBRID DIAGRAM (A) (Figure 7.3) and HYBRID DIAGRAM (B) (Figure 7.4).

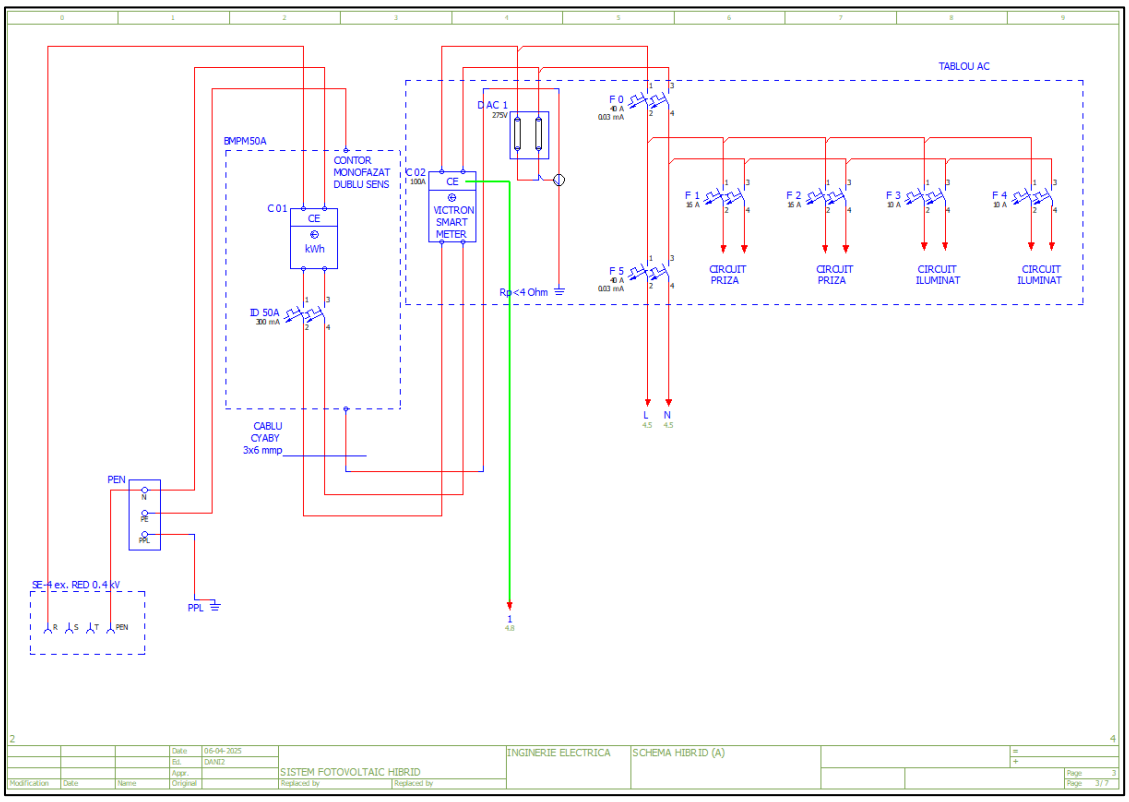


Figure 7.3 Hybrid diagram (A)

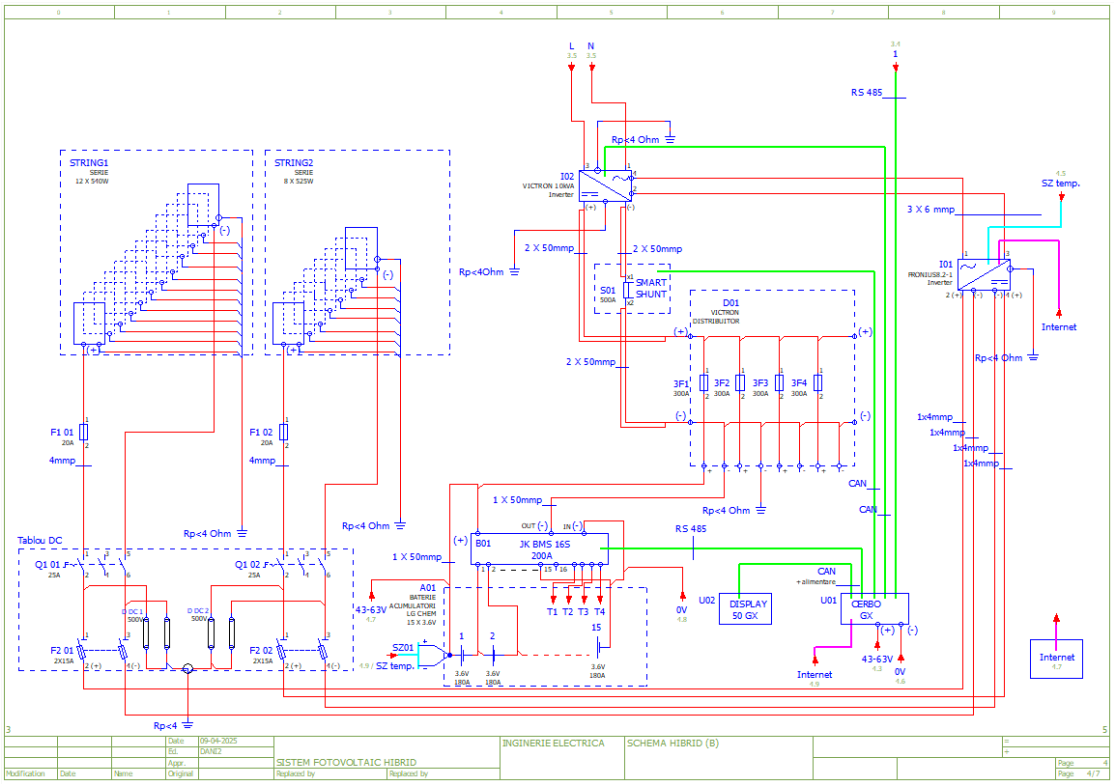


Figure 7.4 Hibrid diagram (B)

Consumers circuits are protected by circuit breakers (*F01 ... F04*), and two other circuit breakers, *F0* and *F5*, are used upstream of them to provide additional protection to the two sources of electricity.

By using the Cerbo GX *U1*, the GX Touch *U2 display, the* S01 *battery charge/ discharge monitoring element*, the *C02 energy meter* and the other monitoring components integrated into the inverters, the system can automatically adjust the power distribution, optimize consumption and reduce dependence on the grid.

If in the case of the on-grid photovoltaic system, the module for converting solar energy into DC energy was represented, in addition to the protection elements, by two strings of 12 photovoltaic panels (*String 1* – 9 pcs, *String 2* – 3 pcs), in the case of the hybrid one, two strings configured as follows are used:

– String 1 consisting of 12 Sharp NU-JD540W photovoltaic panels (Figure 7.5);
– String 2 consisting of 8 Longi LR5-66HTH-525M photovoltaic panels (Figure 7.6).



Figure 7.5 Sharp NU-JD540W 12 panels string



Figure 7.6 Longi LR5-66HTH-525M 8 panels string

In total, the total power of the photovoltaic system is 10.68kWp. The implemented configuration ensures control of the voltage injected into the AC network, helping to prevent the occurrence of overvoltages in the local network and to maintaining the stability of the electrical parameters in the context of load and production variations.

7.3. Choosing the BMS and optimizing the LG Chem 15s3p battery pack

7.3.1. BMS Identification

To ensure the safe and efficient operation of the battery pack, the JK PB2A16S20P management system produced by JIKONG Electronics was selected, due to its high compatibility with configurations of up to 16 cells in series and advanced protection and monitoring functions. It monitors cell voltages and temperatures, prevents imbalances during charge-discharge cycles, and provides multiple protections against overvoltage, over-discharge, short circuit, or overheating. The choice of this BMS for the 15-cell assembly is justified by its ability to handle high currents and the flexibility offered by configuration and integration. The integration of the BMS together with the cell battery in the electrical diagram of the photovoltaic system was carried out through blocks *A01* and *B01*.

Experimentally, the aim was to connect the balance wires of the BMS. They are attached to each connection point between the groups of cells, following the indicated numbering: B0 will be connected to the negative terminal of the battery, B1 to the first serial connection, and so on, up to B15, which connects to the positive terminal of the last group. Finally, the main terminals were also connected:

- the negative battery terminal (marked *B*-) connects directly to the BMS;
- the *P- terminal*, which comes out of the BMS, is the one that will connect to the hybrid inverter;
- the positive terminal of the battery (marked *B*+) will connect to the same inverter, without going through the BMS.

Also, temperature monitoring is done with the help of T1 sensors ... T4 of the BMS together with the *SZ01* sensor of the hybrid inverter connected to the *B+ terminal* of the battery. Figure 7.7 shows the interconnection between the BMS and the configuration of the 15s3p battery pack. At the same time, the assembly of the section of the added electrical elements is identified in Figure 7.8.

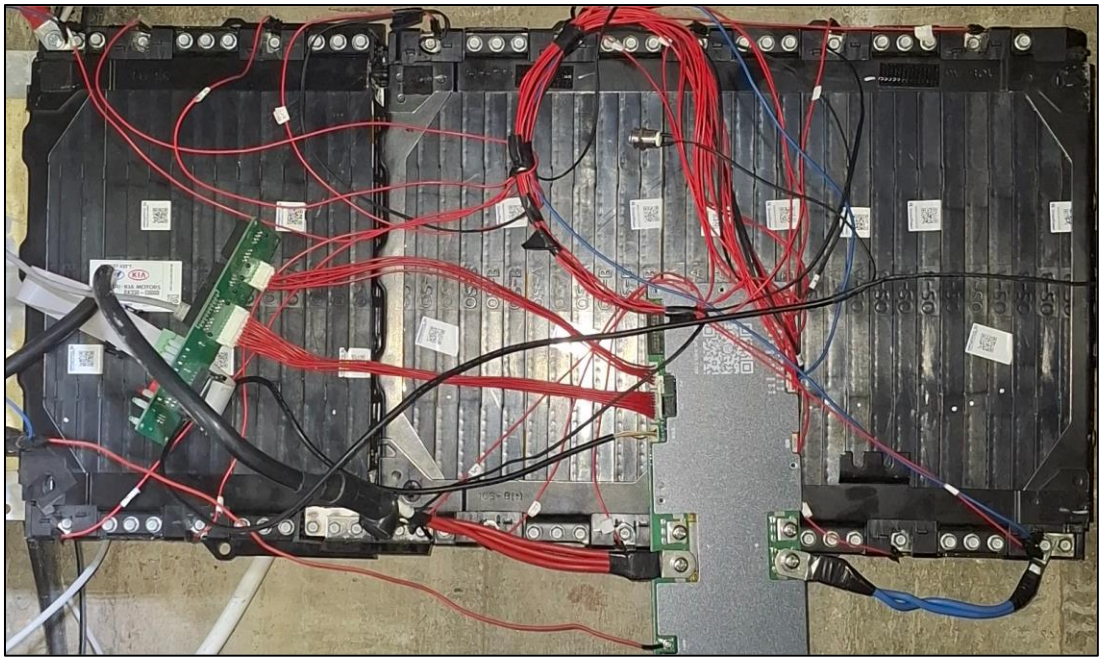


Figure 7.7 BMS - battery interconnection



Figure 7.8 Installation of the section of additional electrical elements

7.3.2. Determination of the optimal loading/unloading parameters and analysis of the obtained data

The static test applied to the LG Chem 58.4Ah cell aims to determine the optimal loading and discharging thresholds, using the EBC-A40L equipment and the standard CC-CV algorithms for charging and DC for discharging. The procedure involves controlled constant current cycles, with voltage limits set at 4.2 for charging and 2.5V for discharging, following the *USABC Test Procedures Manual* methodology (rev. 3.1, 2020).

The cell undergoes a preliminary training cycle designed to stabilize electrochemically and eliminate the influence of the history of use. This cycle consists of the complete discharge of the cell up to the voltage of 2.5V followed by a one-hour break for electrochemical stabilization. Subsequently, the cell is fully charged up to 4.2V with a constant current of 19.4A

and a limitation of the current absorbed in the CV stage to 2.9A. After reaching the voltage of 4.2V and completing the current absorption, a new one-hour break is applied, also to achieve thermal and electrochemical balance.

The experimental results showed a stable overlap of the loading and unloading curves, which confirms the reproducibility of the tests. From the recorded data, the following can be seen (Figure 7.9):

– after the value of 3.30V towards the minimum discharge threshold proposed by the manufacturer of the LG Chem cell (2.50V), the curve becomes very steep, which demonstrates a battery stress in the range of 2.50 – 3.30V;

– above the value of 4.10V, towards the maximum charge value indicated by the manufacturer (4.20V), the charge curve attempts a more pronounced rise in a short period of time, which proves another stress to which the cell is subjected during discharge.

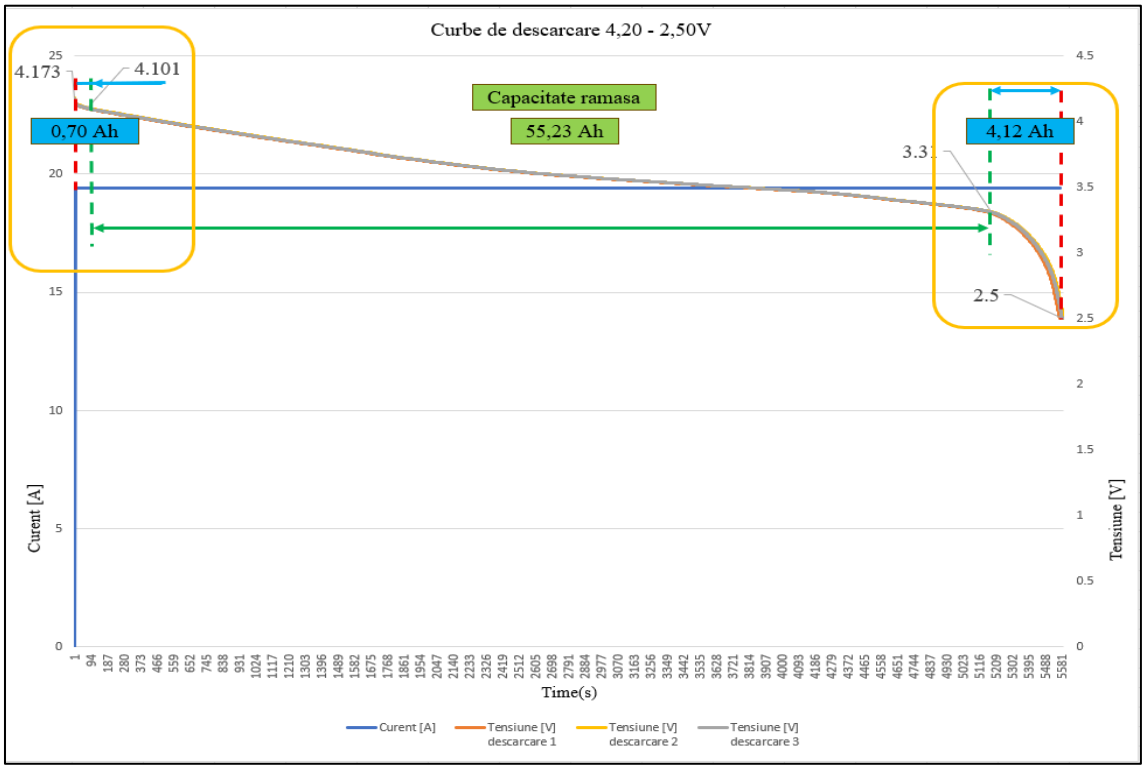


Figure 7.9 Calculation of capacities for proposed thresholds

Table 7.1 highlights the capacity values calculated on the chosen ranges:

Table 7.1 Capacity values on the chosen discharge intervals

Electrical voltage interval [V]	2.50 - 4.20	2.50 - 3.30	3.30 - 4.10	4.10 - 4.20
Capacity [Ah]	60.02	4.12	55.23	0.70

.

Therefore, the use of 3.30V discharge and 4.10V load thresholds is recommended in applications that focus on the durability of cells in repeated cyclic regimes, especially in the context of their reuse for renewable energy storage. This achieves a justified compromise between performance and wear, losing approximately 9.34Ah (15.7%) of capacity, but significantly protecting the chemical integrity of the electrodes.

Chapter 8

Determining the degree of wear of the second-life battery before and after integration into the photovoltaic system

8.1. General principles for evaluating the electrical performance of the second-life battery

Evaluation of electrical performance is necessary in the case of second-life batteries, as they are intended for different uses than the original applications. After use in electric vehicles, batteries can be reconfigured for different applications, where power and cyclicity requirements are less demanding. Reference manuals, such as the *USABC Test Procedures Manual* [41], contain the procedures necessary to evaluate the performance of batteries, which apply to all types of batteries and therefore do not specify the necessary equipment used in the tests, but only the physical quantities to be tracked and recorded: voltage, current, power and temperature. The most common testing methods include:

- static capacity test;
- hybrid pulse power characterization test (HPPC)
- test for determining internal impedance (Electrochemical impedance spectroscopy)

8.2. Presentation of laboratory equipment "Battery testing"

The "Battery Testing" laboratory was carried out within the Sectoral Operational Program Increasing Economic Competitiveness, priority axis 2: Competitiveness through research – development and innovation, D2.2: Investments in RDI infrastructure and development of administrative capacity, through the project entitled “CENTRUL REGIONAL DE CERCETARE–DEZVOLTARE PENTRU MATERIALE, PROCESE și PRODUSE INOVATIVE DESTINATE INDUSTRIEI DE AUTOMOBILE (CRC&D-Auto)” 2015.

For the evaluation of the electrical performance of the second-life battery used, the following equipment was used in the "Battery Testing" laboratory:

- thermal camera model MRC
- battery impedance meter Hioki Battery Impedance Meter BT4560 1050Hz
- battery charge and discharge test software (Chroma Battery)
- multifunctional test system EBC A40L

8.3. Static Capacity Test

From the batch selected for integration into the photovoltaic system, consisting of 15 modules, each consisting of 3 cells of the same type, 5 cells were selected for the evaluation of the performance of the batteries with the help of the tests presented in section 8.1. These tests were carried out both at the purchase of the cells and after their use in the photovoltaic system, for 12 months. The selection aimed to obtain a representative sample, suitable for a preliminary analysis of the electrochemical behavior under controlled conditions. This choice contributes to the objectivity of the testing and allows the evaluation of performance variations between cells from the same manufacturing batch.

For this test, the EBC A40L multifunctional test system was used together with the dedicated EB Tester Software (Figure 8.1).



Figure 8.1 Equipment used to perform the static capacity test

➢ *Test conditions*

The experimental tests were carried out in accordance with the following standardized conditions, in accordance with the manufacturer's specifications:

– ambient temperature: 25°C ± 2°C, provided by the local air conditioning system;

– the loading of the cell was carried out according to the algorithm specified by the manufacturer;

– after each charge/discharge cycle, a rest period of at least 60 minutes was introduced for thermal and electrochemical stabilization of the cell;

– during the tests, current, voltage and time were continuously monitored via the data acquisition system.

➢ *Procedure de test*

The test procedure was preceded by a process of preparation of the cells, consisting of a preliminary stabilization cycle, carried out as follows:

– complete discharge of the cell up to the voltage of 2.50V;

– 60-minute stabilization break;
– full cell charging up to the maximum voltage of 4.20V;
– 60-minute stabilization break.

After the preparation phase, the static test itself was carried out over three complete cycles, each consisting of a discharge phase followed by a loading phase, as follows:

– the discharge was carried out immediately after the break, at a constant current of 19.40A (corresponding to a C/3 regime in relation to the nominal capacity);
– the discharge was carried out until the minimum voltage of 2.50V was reached;
– after each discharge, a 60-minute break was made for thermal and electrochemical stabilization;
– cell charging has been achieved up to the maximum operating voltage of 4.20V;
– the charging was carried out with a constant current regime of 19.40A followed by constant voltage (DC-CV), respecting the specific load profile;
– the process was repeated three times and the results were compared to check the stability of the.

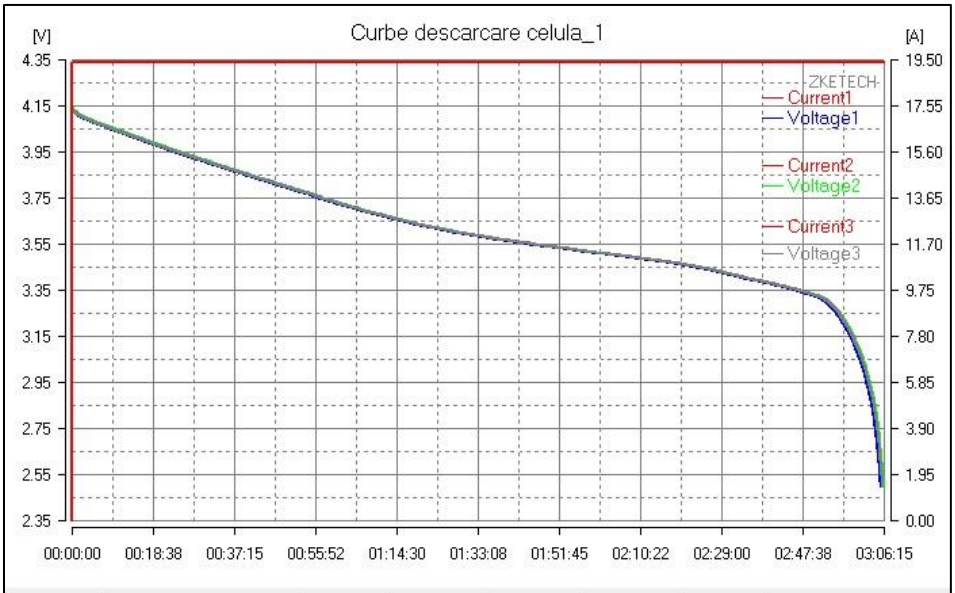
➢ *Analysis and interpretation of results*

The capacitance values obtained from each test cycle were extracted from the discharge curves for each cell.

8.3.1. Static capacity test when purchasing cells

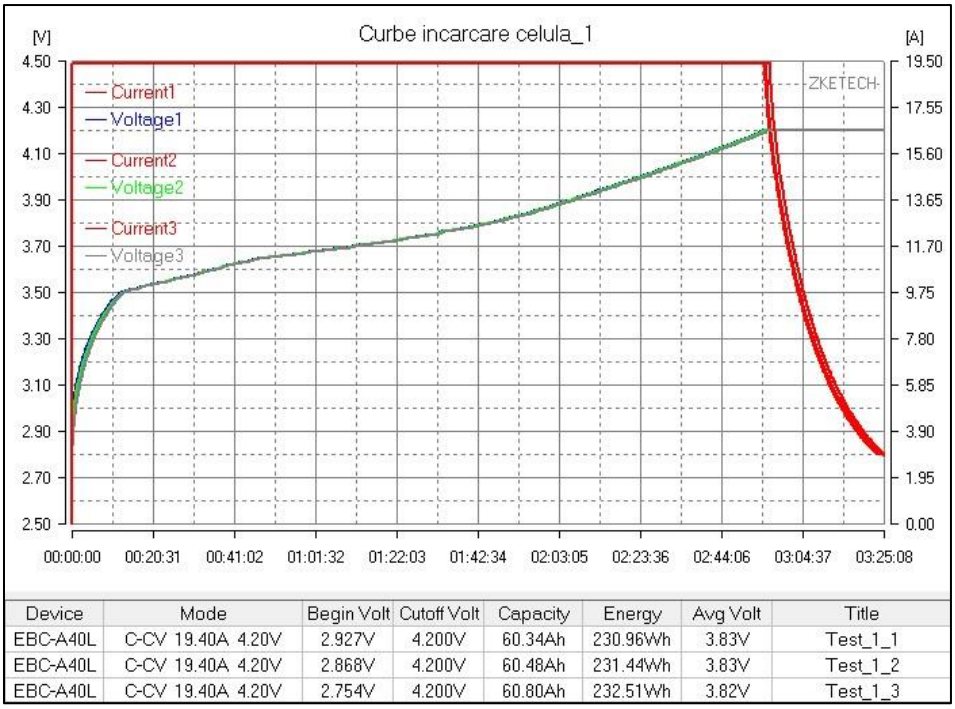
Three discharge curves and three charge curves were obtained for each of the five selected cells, following tests carried out at the time of purchase, before integration into the photovoltaic system:

– Cell 1 – discharge curves (Figure 8.2) and load curves (Figure 8.3)



Device	Mode	Begin Volt	Cutoff Volt	Capacity	Energy	Avg Volt	Title
EBC-A40L	D-CC 19.40A 2.50V	4.173V	2.500V	60.00Ah	217.01Wh	3.62V	Test_1_1
EBC-A40L	D-CC 19.40A 2.50V	4.177V	2.500V	60.23Ah	218.01Wh	3.62V	Test_1_2
EBC-A40L	D-CC 19.40A 2.50V	4.173V	2.500V	60.14Ah	217.65Wh	3.62V	Test_1_3

Figure 8.2 cell 1 discharge curves



Device	Mode	Begin Volt	Cutoff Volt	Capacity	Energy	Avg Volt	Title
EBC-A40L	C-CV 19.40A 4.20V	2.927V	4.200V	60.34Ah	230.96Wh	3.83V	Test_1_1
EBC-A40L	C-CV 19.40A 4.20V	2.868V	4.200V	60.48Ah	231.44Wh	3.83V	Test_1_2
EBC-A40L	C-CV 19.40A 4.20V	2.754V	4.200V	60.80Ah	232.51Wh	3.82V	Test_1_3

Figure 8.3 cell 1 charging curves

The arithmetic average of the discharged capacity values obtained in the three measurements is 60.12Ah, and the maximum deviation from this value is below the threshold of ±2% (range: 58.92Ah – 61.32Ah). All three capacity values fall within this range, which confirms the stability of the results and the validation of the test (Table 8.1).

Table 8.1 Cell 1 – Static Capability Test Validation

Test	Discharged capacity (Ah)	Deviation from the average (Ah)	Relative deviation (%)
1	60.00	-0.12	0.20%
2	60.23	+0.11	0.18%
3	60.14	+0.02	0.03%

– Cell 2 – the data obtained are summarized in Table 8.2:

The arithmetic average of the discharged capacity values obtained in the three measurements is 59.99Ah, and the maximum deviation from this value is below the threshold of ±2% (range: 58.79Ah – 61.19Ah). All three capacity values fall within this range, which confirms the stability of the results and the validation of the test.

Table 8.2 Cell 2 – Static Capability Test Validation

Test	Discharged capacity (Ah)	Deviation from the average (Ah)	Relative deviation (%)
1	59.72	-0.27	0.45%
2	60.05	+0.06	0.10%
3	60.20	+0.21	0.35%

– Cell 3 – the data obtained are summarized in Table 8.3:

The arithmetic average of the values of the discharged capacity obtained within the three measurements is 60.11Ah, and the maximum deviation from this value is below the threshold of ±2% (range: 58.91Ah – 61.31Ah). All three capacity values fall within this range, which confirms the stability of the results and the validation of the test.

Table 8.3 Cell 3 – Static Capability Test Validation

Test	Discharged capacity (Ah)	Deviation from the average (Ah)	Relative deviation (%)
1	59.95	-0.16	0.27%
2	60.06	-0.05	0.08%
3	60.33	+0.22	0.37%

– Cell 4 – the data obtained are summarized in Table 8.4:

The arithmetic average of the discharged capacity values obtained in the three measurements is 59.64Ah, and the maximum deviation from this value is below the threshold of ±2% (range: 58.45Ah – 60.83Ah). All three capacity values fall within this range, which confirms the stability of the results and the validation of the test.

Table 8.4 Cell 4 – Static Capacity Test Validation

Test	Discharged capacity (Ah)	Deviation from the average (Ah)	Relative deviation (%)
1	59.67	+0.03	0.05%
2	59.65	+0.01	0.01%
3	59.60	-0.04	0.06%

– Cell 5 – the data obtained are summarized in Table 8.5:

The arithmetic mean of the values of the discharged capacity obtained within the three measurements is 59.88Ah, and the maximum deviation from this value is below the threshold of ±2% (range: 58.68Ah – 61.08Ah). All three capacity values fall within this range, which confirms the stability of the results and the validation of the test.

Table 8.5 Cell 5 – Static Capacity Test Validation

Test	Discharged capacity (Ah)	Deviation from the average (Ah)	Relative deviation (%)
1	59.76	-0.12	0.20%
2	59.85	-0.03	0.05%
3	60.02	+0.14	0.23%

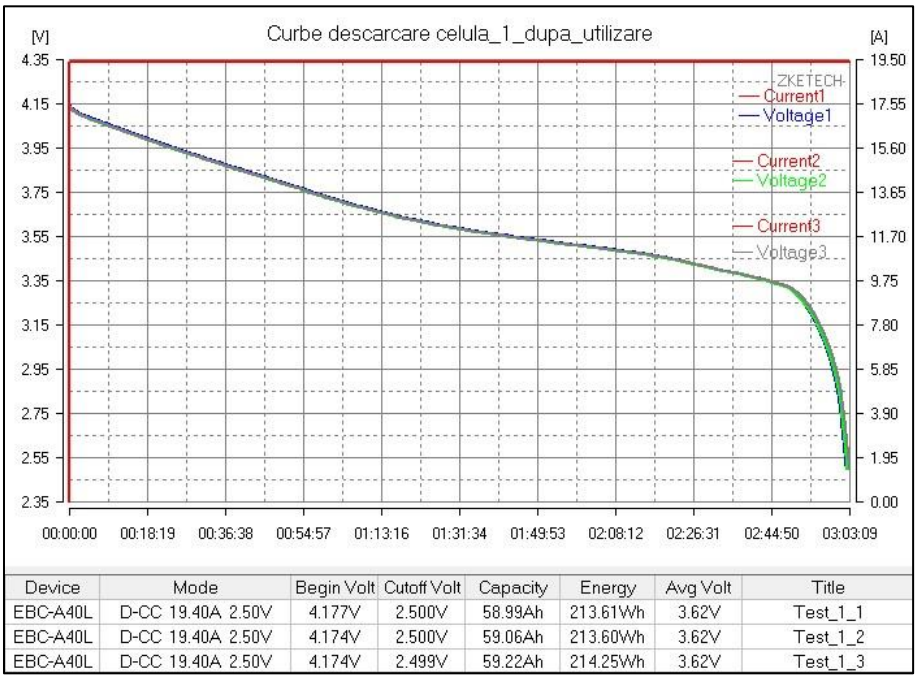
The results obtained from the static capacity tests for the five cells analyzed indicate their electrochemical stability and a uniformity of the charge-discharge process. The values of the discharged capacity fall within the validation range of ±2% compared to the arithmetic average, with maximum relative deviations of 0.20% – 0.45%. Also, the charged capacity was consistently higher than the discharged capacity, which can be explained by the inherent losses

in electrochemical and resistive processes. Given the uniformity of the values and the low deviation from the average, the tests can be considered valid and the data obtained can be used as reference values in the subsequent evaluation of the performance of the cells.

8.3.2. Static capacity test after use in PV system

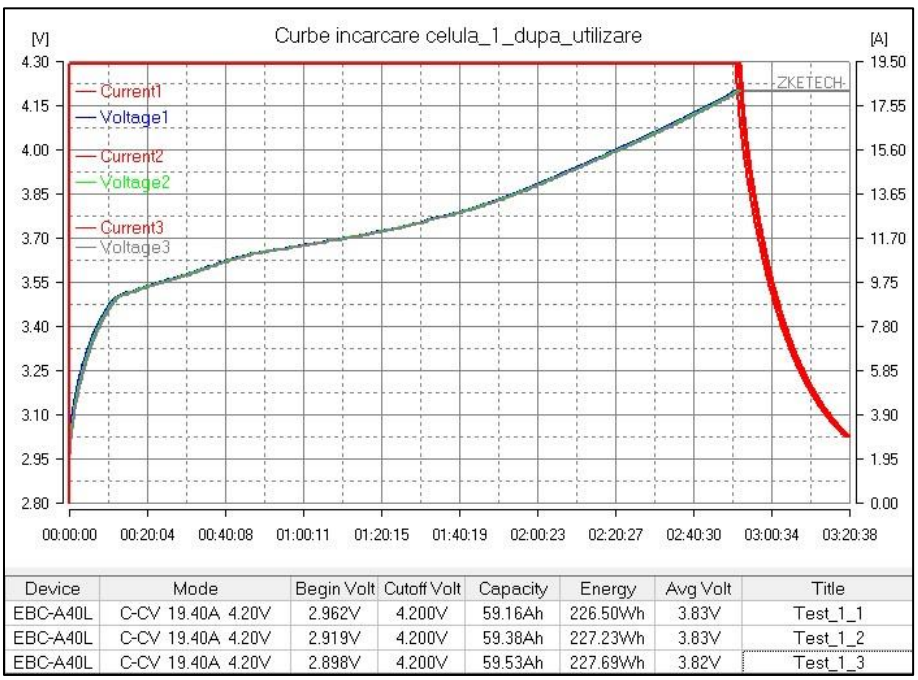
After 12 months of operation in the photovoltaic system, the same 5 cells were subjected to the static capacity test, obtaining the following curves:

– Cell 1 – discharge curves (Figure 8.4) and load curves (Figure 8.5)



Device	Mode	Begin Volt	Cutoff Volt	Capacity	Energy	Avg Volt	Title
EBC-A40L	D-CC 19.40A 2.50V	4.177V	2.500V	58.99Ah	213.61Wh	3.62V	Test_1_1
EBC-A40L	D-CC 19.40A 2.50V	4.174V	2.500V	59.06Ah	213.60Wh	3.62V	Test_1_2
EBC-A40L	D-CC 19.40A 2.50V	4.174V	2.499V	59.22Ah	214.25Wh	3.62V	Test_1_3

Figure 8.4 cell 1 discharge curves after use



Device	Mode	Begin Volt	Cutoff Volt	Capacity	Energy	Avg Volt	Title
EBC-A40L	C-CV 19.40A 4.20V	2.962V	4.200V	59.16Ah	226.50Wh	3.83V	Test_1_1
EBC-A40L	C-CV 19.40A 4.20V	2.919V	4.200V	59.38Ah	227.23Wh	3.83V	Test_1_2
EBC-A40L	C-CV 19.40A 4.20V	2.898V	4.200V	59.53Ah	227.69Wh	3.82V	Test_1_3

Figure 8.5 cell 1 charging curves after use

The arithmetic average of the discharged capacity values obtained within the three measurements is 59.09Ah, and the maximum deviation from this value is below the threshold of ±2% (range: 57.91Ah – 60.27Ah). All three capacity values fall within this range, which confirms the stability of the results and the validation of the test (Table 8.6).

Table 8.6 Cell 1 after use – static capability test validation

Test	Discharged capacity (Ah)	Deviation from the average (Ah)	Relative deviation (%)
1	58.99	-0.10	0.17%
2	59.06	-0.03	0.05%
3	59.22	+0.13	0.22%

– Cell 2 – the data obtained are summarized in Table 8.7:

The arithmetic mean of the discharged capacity values obtained within the three measurements is 58.96Ah, and the maximum deviation from this value is below the threshold of ±2% (range: 57.78Ah – 60.14Ah). All three capacity values fall within this range, which confirms the stability of the results and the validation of the test.

Table 8.7 Cell 2 after use – static capacity test validation

Test	Discharged capacity (Ah)	Deviation from the average (Ah)	Relative deviation (%)
1	58.84	-0.12	0.20%
2	59.00	+0.04	0.07%
3	59.04	+0.08	0.14%

– Cell 3 – the data obtained are summarized in Table 8.8:

The arithmetic average of the discharged capacity values obtained in the three measurements is 59.01Ah, and the maximum deviation from this value is below the threshold of ±2% (range: 57.83Ah – 60.19Ah). All three capacity values fall within this range, which confirms the stability of the results and the validation of the test.

Table 8.8 Cell 3 after use – static capacity test validation

Test	Discharged capacity (Ah)	Deviation from the average (Ah)	Relative deviation (%)
1	58.84	-0.17	0.29%
2	59.07	+0.06	0.10%
3	59.13	+0.12	0.20%

– Cell 4 – the data obtained are summarized in Table 8.9:

The arithmetic average of the discharged capacity values obtained in the three measurements is 58.90Ah, and the maximum deviation from this value is below the threshold of ±2% (range: 57.72Ah – 60.08Ah). All three capacity values fall within this range, which confirms the stability of the results and the validation of the test.

Table 8.9 Cell 4 after use – Static Capability Test Validation

Test	Discharged capacity (Ah)	Deviation from the average (Ah)	Relative deviation (%)
1	58.74	-0.16	0.27%
2	58.87	-0.03	0.05%
3	59.09	+0.19	0.32%

– Cell 5 – the data obtained are summarized in Table 8.10:

The arithmetic average of the values of the discharged capacity obtained within the three measurements is 58.99Ah, and the maximum deviation from this value is below the threshold of ±2% (range: 57.81Ah – 60.17Ah). All three capacity values fall within this range, which confirms the stability of the results and the validation of the test.

Table 8.10 Cell 5 after use – Static Capability Test Validation

Test	Discharged capacity (Ah)	Deviation from the average (Ah)	Relative deviation (%)
1	58.82	-0.17	0.29%
2	58.97	-0.02	0.03%
3	59.19	+0.20	0.34%

8.3.3. Analysis and conclusions

The analysis of static capacity tests highlights the electrochemical behavior of the cells in two distinct stages: before and after use for 12 months in real operation (Figure 8.6). By comparing the values of the discharged capacity in both cases, the aim was to identify any functional degradations, which can be quantitatively expressed by decreasing the available capacity.

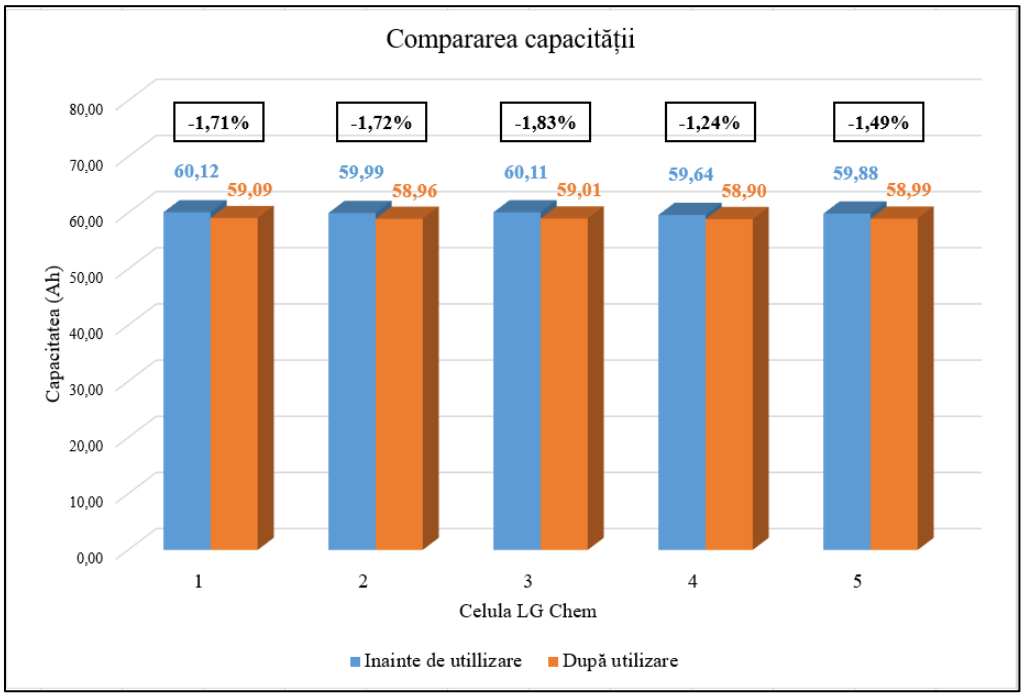


Figure 8.6 Comparison of cell capacity before and after use

In the initial stage, all five cells showed capacity values located in the vicinity of the nominal value of 60Ah, with a low relative dispersion (below ±0.5% compared to the arithmetic average), which confirms the homogeneity of the batch and the quality of the manufacturing process. The discharged capacity values were consistent between the three cycles for each cell, and the relative deviations from the mean remained well below the validation threshold of ±2%, indicating good stability and repeatability of the test.

After 12 months of use in the PV system, a slight decrease in capacity was observed for all cells tested. The average discharged capacity decreased by about 0.9 – 1.1Ah compared to the initial values, which corresponds to a relative loss of about 1.2 – 1.8%. This moderate degradation does not indicate the appearance of accelerating wear phenomena. In addition, the values of the post-use capacities continue to fall within the validation intervals defined by the deviation of ±2% from the individual arithmetic mean, which confirms the maintenance of electrochemical coherence and the operation of the cell within stable parameters.

Therefore, the data obtained from the static test support the idea that the analyzed cells can be considered suitable for photovoltaic energy storage applications, even after an operating period of 12 months. This result reflects a slow and uniform degradation, characteristic of a stable electrochemical behavior under real operating conditions.

8.4. Hybrid Pulse Power Characterization Test - HPPC

To perform this test, the Chroma Battery Charge/ Discharge test software is used together with the Chroma 62000P series programmable DC power supply and the Chroma 63100A series programmable DC load (Figure 8.7).



Figure 8.7 Equipment used to perform the HPPC test

As the Chroma Battery Charge has limitations that do not allow the application of impulse currents according to the maximum requirements (such as the charging current of 43.8A for 0.75C), a scaling of the test profiles was resorted to. Thus, the tests were carried out

with a discharge current of 40A and a charging current of 30A. This approach is allowed according to the *USABC Test Procedures Manual*, which specifies that tests can be scaled proportionally provided that the test profile and analysis methodology are maintained. The objective of this scaling was to preserve the test form for the characterization of the impulse resistance and power capability of the cell, under the conditions of an operating regime adapted to the laboratory equipment.

- *Test conditions*

The experimental tests will be carried out in compliance with the following standardized conditions, in accordance with the manufacturer's specifications:

– ambient temperature: 25°C ± 2°C, provided by the thermal chamber in the laboratory;
– charging the cell according to the algorithm specified by the manufacturer;
– after each full charge and discharge cycle, as well as after each HPPC pulse, a minimum of 60 minutes of rest will be introduced for stabilization;
– during the tests, current, voltage and time will be continuously monitored via the data acquisition system.

- *Procedure de test*

The test procedure will be preceded by a cell preparation process, consisting of a preliminary stabilization cycle. After the preparation stage, the HPPC test itself will be performed according to the methodology specified in the *USABC Test Procedures Manual*. Starting from a fully charged state, a standard HPPC profile is applied.

Table 8.11 presents the simplified structure of an HPPC profile followed by 10% capacity discharge, in relation to the equipment used. The applied current is considered positive on discharge and negative on charge.

Table 8.11 Structure of an HPPC test profile + 10% capacity discharge

Step	Sequence	Equipment	Time	Setting
1	discharge	DC source Chroma 62000P	30s	CC = 40A
2	brake	-	40s	off
3	charge (regen)	DC load Chroma 63100A	10s	CC = -30A
4	discharge	DC source Chroma 62000P	1509s	CC = 13,33A
5	break	-	3600s	off

This cycle (pulses + C/3 discharge + rest) is repeated until at least 90% DOD is reached, with measurements taken at each intermediate stage (90%, 80%, ..., 10% SOC). For each pulse, current, voltage, and time are recorded, using which the pulse resistance and pulse power capability are determined, according to the methodology in Section 4.4 of the *USABC Test Procedures Manual*.

8.4.1. HPPC Test When Purchasing Cells

In the context of the present study, the HPPC test was carried out in a controlled regime according to the *USABC Test Procedures Manual methodology*, using the Chroma 62000P programmable source and the Chroma 6310A downloader, with control through the software interface on the laptop. During some pulse sequences, interruptions occurred in the

communication between the equipment and the control interface, which led to the loss of the active control and the impossibility of correctly applying the current/voltage profile. In the absence of a controlled shutdown, out of the 5 cells tested after use in the photovoltaic system, 3 cells exceeded the operating limits imposed by the protocol (minimum discharge voltage, respectively before/after pulse rest conditions), which generated thermal and electrochemical deviations that compromise the integrity and subsequent repeatability of the measurements. For this reason, the test became destructive for the 3 cells invalidating their subsequent use in comparative evaluations.

This incident highlights both the sensitivity of the HPPC test to the integrity of the communication chain and compliance with stability windows, as well as the need for continuous surveillance throughout the protocol (≈25 hours/cell). As a result, the extension of testing to all five cells originally proposed was abandoned and a restrictive sampling strategy was adopted, limited to the two remaining functional cells, selected to preserve the representativeness of the batch. The statistical justification was made in relation to the principles of ISO 2859-1, with the definition of non-compliance as non-fulfillment of the HPPC eligibility conditions.

- Cell 1 before use – HPPC test sequence (Figure 8.8)

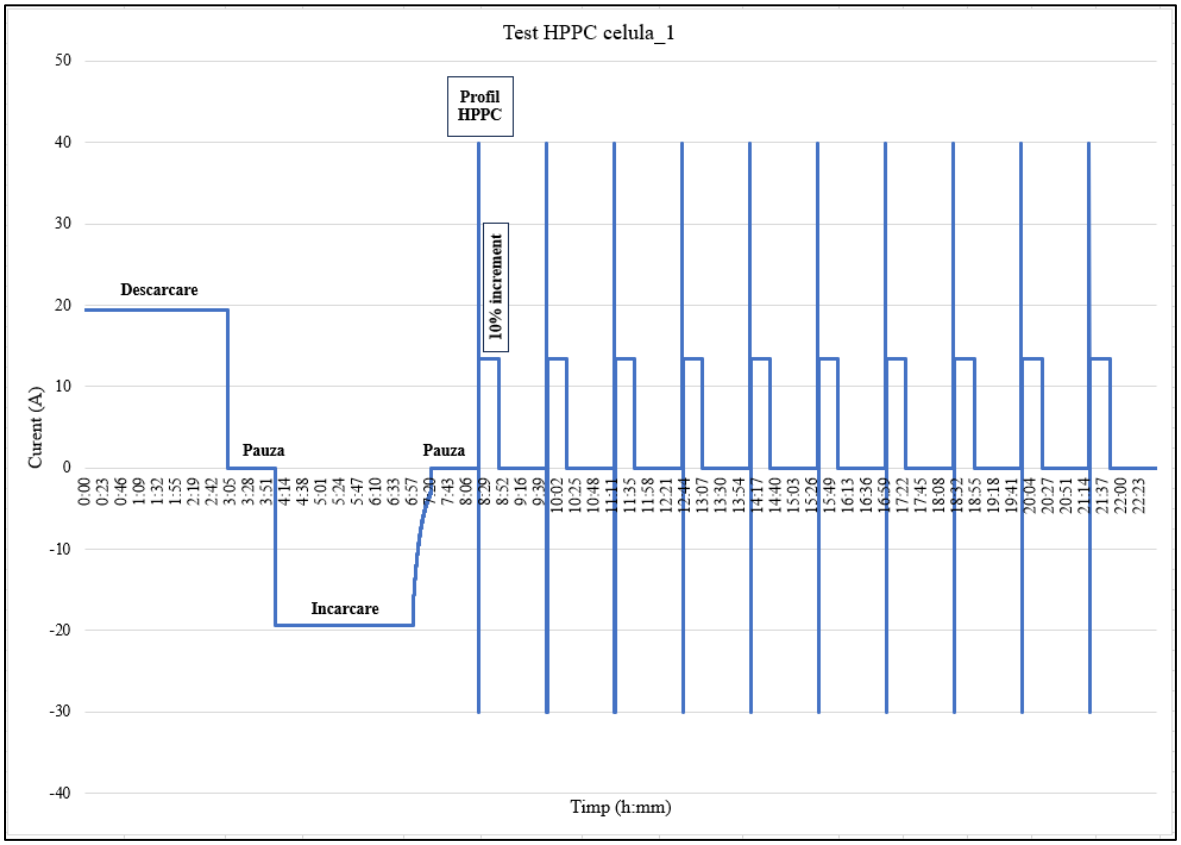


Figure 8.8 HPPC test – cell 1 before use

Figure 8.9 illustrates how the internal resistance at each discharge/charge pulse varies depending on the charge state of the cell. The analysis of the evolution of the internal resistance is performed by applying a polynomial fit of order 3 (polynomial fit) using the *Polynomial Trendline* function in Microsoft Excell.

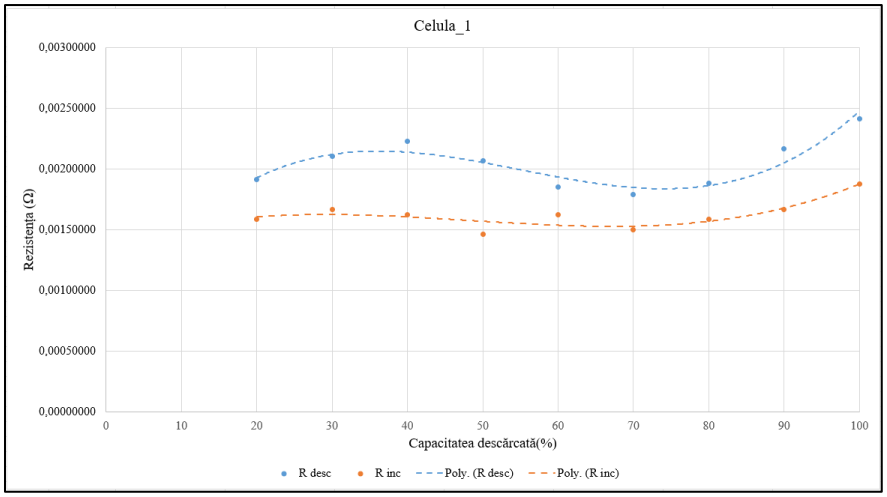


Figure 8.9 Impulse resistance as a function of discharged capacity – cell 1 before use

- Cell 2 before use

Figure 8.10 shows how the internal resistance at each discharge/charge pulse changes as the charge state of the cell decreases.

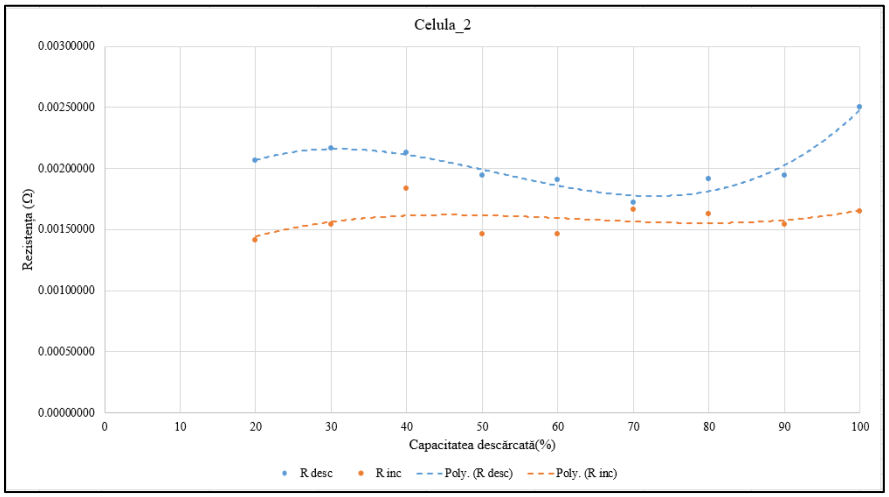


Figure 8.10 Impulse resistance as a function of discharged capacity – cell 2 before use

8.4.2. HPPC test after use in PV system

After 12 months of operation in the PV system, the same five cells were subjected to the HPPC test again, resulting in the following:

- Cell 1 after use – HPPC test (Figure 8.11)

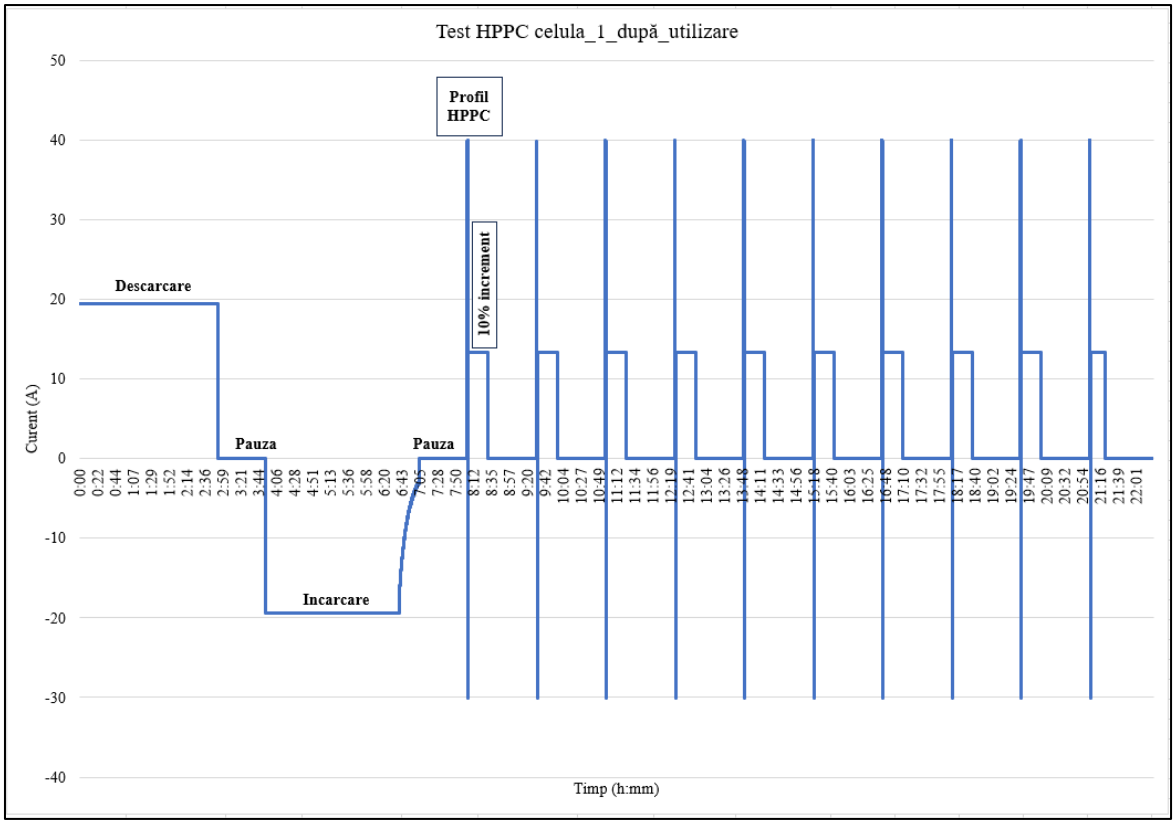


Figure 8.11 HPPC test – cell 1 after use

Figure 8.12 illustrates how the internal resistance at each discharge/charge pulse changes as the charge state of the cell decreases.

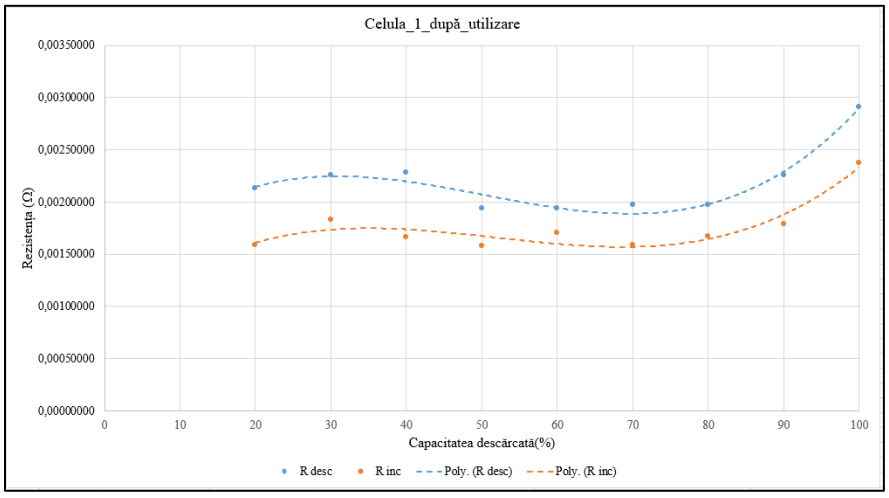


Figure 8.12 Impulse resistance as a function of discharged capacity – cell 1 after use

- Cell 2 after use

Figure 8.13 shows how the internal resistance to each discharge/charge pulse changes as the charge state of the cell decreases.

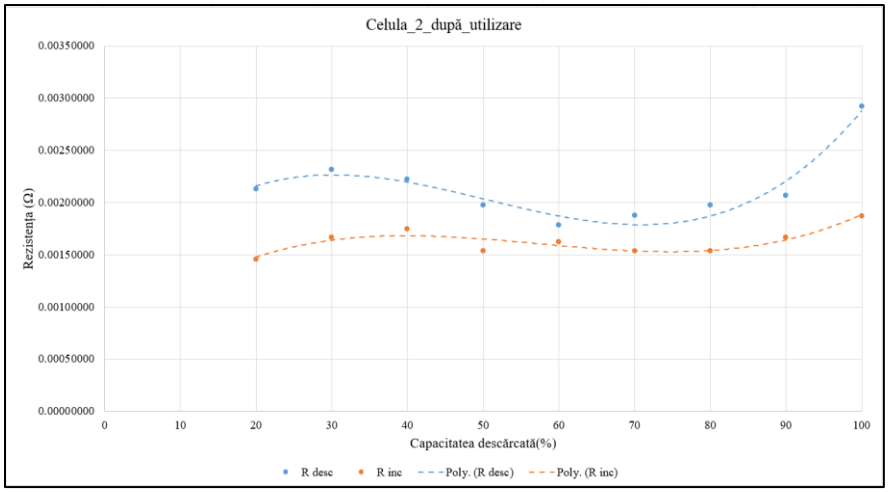


Figure 8.13 Impulse resistance as a function of discharged capacity – cell 2 after use

8.4.3. Analysis and conclusions

The comparative analysis of the internal resistance to discharge and charge, before and after use, for cells 1 and 2, highlights important differences in the degradation of electrochemical parameters following the operating cycles (Table 8.12, Table 8.13).

Table 8.12 Internal resistance before and after use according to discharged capacity – cell 1

Discharged capacity (%)	R_{desc} (mΩ) before use	R_{desc} (mΩ) after use	ΔR_{desc} (%)	$R_{înc}$ (mΩ) Before use	$R_{înc}$ (mΩ) after use	$\Delta R_{înc}$ (%)
10	-	-	-	-	-	-
20	1.9098	2.1328	11.68	1.5828	1.5861	0.21
30	2.1003	2.2556	7.39	1.6661	1.8327	10.00
40	2.2231	2.2882	2.93	1.6228	1.6661	2.67
50	2.0677	1.9398	-6.19	1.4595	1.5828	8.45
60	1.8496	1.9423	5.01	1.6228	1.7094	5.34
70	1.7870	1.9724	10.37	1.4995	1.5861	5.78
80	1.8797	1.9749	5.06	1.5828	1.6694	5.47
90	2.1629	2.2556	4.29	1.6661	1.7927	7.60
100	2.4135	2.9148	20.77	1.8760	2.3725	26.47

For cell 1, in discharge mode, the relative increases in internal resistance range between 2.93% and 20.77%, with a pronounced maximum at 100% discharged capacity, which indicates the accumulation of accentuated aging effects in the full discharge zone. A notable exception occurs at 50% discharged capacity, where there is a decrease of 6.19%, possibly associated with uniform redistribution of lithium ions or local changes in the internal structure. Under load, cell 1 shows more pronounced increases at high values of discharged capacity, with a maximum of 26.47% at 100% discharge. In the range of 50–90%, the variations are moderate (5–10%), reflecting a progressive degradation of the load transfer properties, with an impact on the efficiency of energy storage.

Table 8.13 Internal resistance before and after use according to discharged capacity – cell 2

Discharged capacity (%)	R_{desc} (mΩ) before use	R_{desc} (mΩ) after use	ΔR_{desc} (%)	$R_{înc}$ (mΩ) before use	$R_{înc}$ (mΩ) after use	$\Delta R_{înc}$ (%)
10	-	-	-	-	-	-
20	2,0677	2,1328	3,15	1,4162	1,4562	2,82
30	2,1629	2,3183	7,18	1,5428	1,6661	7,99
40	2,1303	2,2255	4,47	1,8327	1,7494	-4,55
50	1,9424	1,9749	1,67	1,4595	1,5395	5,48
60	1,9097	1,7845	-6,56	1,4595	1,6228	11,19
70	1,7218	1,8797	9,17	1,6661	1,5395	-7,60
80	1,9123	1,9749	3,27	1,6261	1,5395	-5,33
90	1,9449	2,0677	6,31	1,5395	1,6661	8,22
100	2,5063	2,9248	16,70	1,6528	1,8727	13,30

For cell 2, the internal discharge resistance analysis shows increases in most discharged capacity ranges, with values between +1.67% and +16.70%. The maximum increase occurs at 100% discharged capacity, which indicates a pronounced impact of aging in the full discharge area. However, there is also a significant decrease to 60% discharged capacity (-6.56%), possibly associated with a more efficient redistribution of lithium ions or a local reorganization of the active material, which temporarily reduces internal resistance. Under load, the variations of the internal resistance are mixed. Increases are observed in the 20–30% and 50–60% ranges, with a maximum of +13.30% at 100% discharged capacity, but also decreases to 40% (-4.55%), 70% (-7.60%) and 80% (-5.33%). These decreases may indicate phenomena of restructuring of the electrode interface or improvement of internal contacts under certain SOC conditions.

Comparatively, cell 1 shows a more uniform degradation, with the predominance of increases in internal resistance in almost all capacitance ranges, indicating a constant aging process of the conductive elements and the electrode interface. Cell 2, on the other hand, shows a more uneven degradation, with alternations between increases and decreases, which suggests a greater sensitivity to operating conditions and more variable evolution of internal parameters.

Overall, for both cells, degradation is more pronounced at high discharged capacities (≥ 90%), where significant increases in internal resistance are observed. This behavior recommends avoiding full discharges and operating the cells within a range of 10–90% discharged capacity, to optimize power performance and extend service life in stationary applications.

Comparison of results showed acceptable internal resistance stability without compromising functionality for stationary applications. These observations support the usability of second-life cells in small-scale energy storage applications with moderate power loads, such as stand-alone or hybrid PV systems.

In conclusion, the use of the HPPC test, even in scaled form, allowed the validation of the performance of cells in stationary storage mode, providing a standardized method for comparative evaluation of degradation and an objective basis for framing cells in second-use applications.

8.5. Test for determining internal impedance - EIS

In order to continue the assessment of the internal degradation of second-life cells after one year of operation in the PV system, EIS measurements were carried out both at the initial and final stages of the period of use. The measurements were made using the HIOKI BT4560 battery impedance tester, an instrument specialized in low-frequency measurements, suitable for the electrochemical characterization of batteries (Figure 8.14).

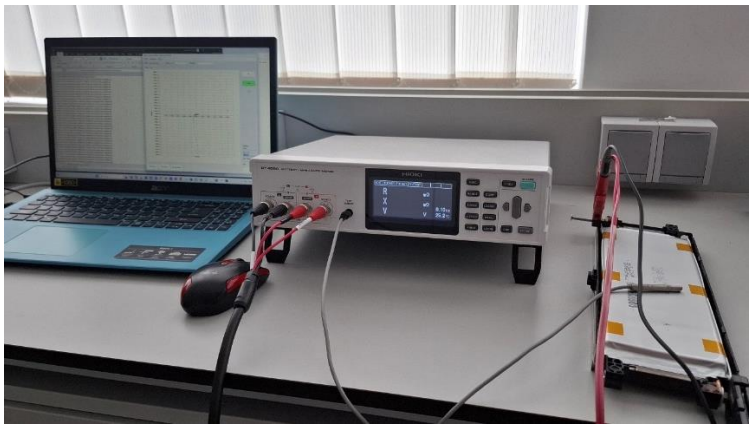


Figure 8.14 Equipment used to perform the EIS test

Tests for the determination of internal impedance are performed starting from a fully charged state, under thermal and electrical rest conditions (SOC stable). Based on measurements made with the Hioki BT4560 equipment, the Nyquist curve is obtained for frequencies between 0.1Hz and 1kHz. This graph provides information about the internal behavior of the cell in the frequency domain, by representing the imaginary component of the impedance according to the real component [42], [43]. The following parameters are extracted:

– ohmic resistance (R_s) – includes the quality of the contacts, the resistance of the electrolyte, the condition of the collectors and an increase in it indicates mechanical degradation;

– total resistance (R_{tot}) – considered the sum of the ohmic resistance and the load transfer resistance and an increase in it indicates an overall internal degradation.

– charge transfer resistance (R_{ct}) – reflects electrochemical processes at the electrode-electrolyte interface.

In a comparative study between the condition of a cell before and after use, monitoring the value of the load transfer resistance R_{ct} is necessary to assess the level of degradation of the electrode-electrolyte interface and to correlate electrochemical wear with performance changes (capacity, energy yield, stability over time) [44]. At the same time, the comparison of R_{tot} values is useful to exclude or isolate contributions of an electrical, mechanical or contact nature, but without providing direct information about internal chemical processes.

8.5.1. EIS test when purchasing cells

The experimental results obtained at this stage are presented and subjected to a detailed analysis, highlighting their implications on the electrochemical behavior of the cells.

➢ Cell 1 before use – Nyquist graph (Figure 8.15)

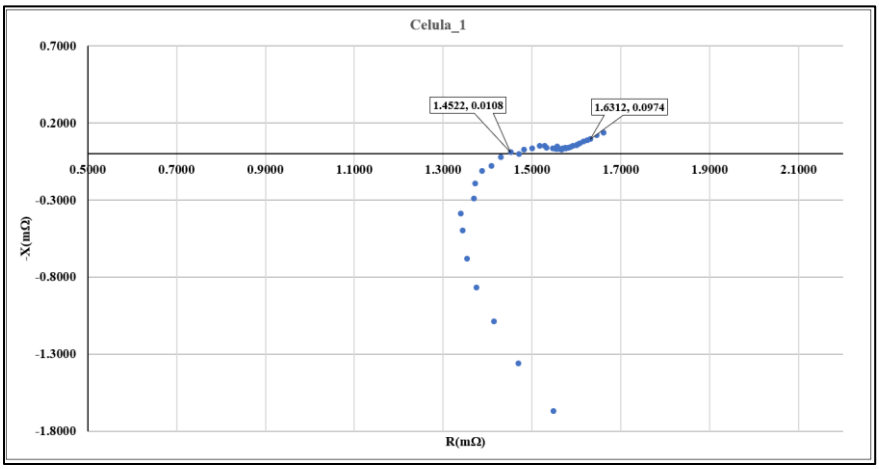


Figure 8.15 Nyquist Chart Cell 1 Before Use

The Nyquist curve obtained for Cell 1 before use reflects typical behavior for a Li-ion cell in a stable electrochemical state. The graph shows a flattened semicircle with no clear elongation in the diffusional region, suggesting an active electrode–electrolyte interface and good ion mobility. The parameters of interest were extracted directly from the experimental data, without adjustments:

- R_s = 1,4522mΩ (50Hz);
- R_{tot} = 1,6312mΩ (0,16Hz);
- R_{ct} = 0,1790mΩ.

➢ Cell 2 before use

For Cell 2 before use, the analysis provides the following parameters:

- R_s = 1,3861mΩ (40Hz);
- R_{tot} = 1,5368 mΩ (0,1Hz);
- R_{ct} = 0,1507mΩ.

➢ Cell 3 before use

For Cell 3 before use, the analysis provides the following parameters:

- R_s = 1,3286mΩ (32Hz);
- R_{tot} = 1,4717mΩ (0,16Hz);
- R_{ct} = 0,1431mΩ.

➢ Cell 4 before use

For Cell 4 before use, the analysis provides the following parameters:

- R_s = 1,3283mΩ (32Hz);
- R_{tot} = 1,4695mΩ (0,16Hz);
- R_{ct} = 0,1412mΩ.

➢ Celula 5 before use

For Cell 5 before use, the analysis provides the following parameters:

- R_s = 1,3547mΩ (32Hz);
- R_{tot} = 1,5309mΩ (0,16Hz);
- R_{ct} = 0,1762mΩ.

8.5.2. EIS test after cell use in the photovoltaic system

Experimental data obtained at this stage:

- Cell 1 after use – Nyquist chart (Figure 8.16)

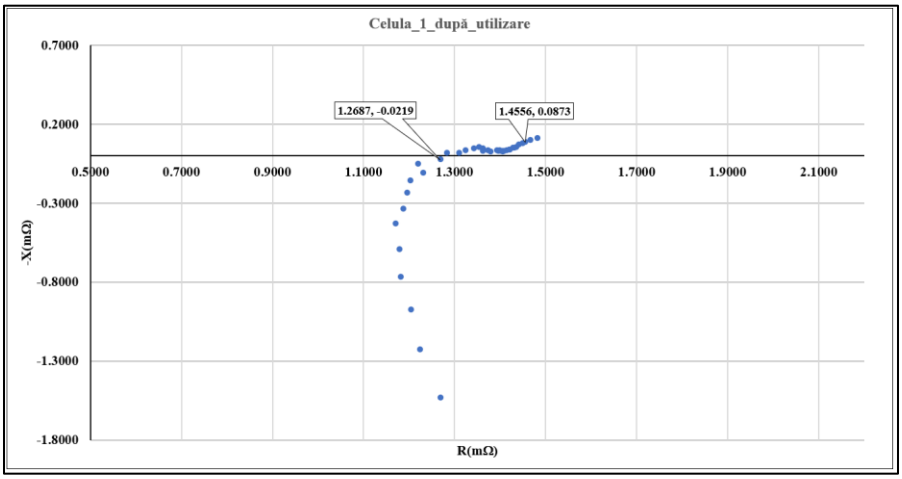


Figure 8.16 Nyquist cell 1 chart after use

For Cell 1 after use, analysis based on the Nyquist curve provides the following:

- R_s = 1,2687mΩ (50Hz);
- R_{tot} = 1,4556mΩ (0,16Hz);
- R_{ct} = 0,1869mΩ.

- Cell 2 after use

For Cell 2 after use, analysis based on the Nyquist curve provides the following:

- R_s = 1,4616mΩ (32Hz);
- R_{tot} = 1,6210mΩ (0,16Hz);
- R_{ct} = 0,1594mΩ.

- Cell 3 after use

For Cell 3 after use, the analysis based on the Nyquist curve provides the following:

- R_s = 1,3279mΩ (40Hz);
- R_{tot} = 1,4842mΩ (0,16Hz);
- R_{ct} = 0,1563mΩ.

- Cell 4 after use

For Cell 4 after use, the analysis based on the Nyquist curve provides the following:

- R_s = 1,3658mΩ (40Hz);
- R_{tot} = 1,5173mΩ (0,16Hz);
- R_{ct} = 0,1515mΩ.

- Cell 5 after use

For Cell 5 after use, analysis based on the Nyquist curve provides the following:

- R_s = 1,3065mΩ (50Hz);
- R_{tot} = 1,4921mΩ (0,16Hz);
- R_{ct} = 0,1856mΩ.

8.5.3. Analysis and conclusions

The objective of this analysis was to highlight, through measurable parameters, the degree of electrochemical degradation accumulated during the use of the cells. The evaluation was carried out by following two specific parameters extracted from the Nyquist curves: the ohmic resistance R_s, associated with the internal resistances of the conductive components of the cell (electrolyte, current collectors, terminals), and the charge transfer resistance R_{ct}, which reflects the difficulty with which the oxidation and reduction processes at the electrode-electrolyte interface are carried out. The results obtained are summarized in the Table 8.14.

Table 8.14 Variation of R_s and R_{ct} for the 5 cells before and after use

Nr. celulă	R_s (mΩ) before use	R_s (mΩ) after use	ΔR_s (%)	R_{ct} (mΩ) before use	R_{ct} (mΩ) after use	ΔR_{ct} (%)
1	1.4522	1.2687	-12.64	0.1790	0.1869	4.41
2	1.3861	1.4616	5.45	0.1507	0.1594	5.77
3	1.3286	1.3279	-0.05	0.1431	0.1563	9.22
4	1.3283	1.3658	2.82	0.1412	0.1515	7.29
5	1.3547	1.3065	-3.56	0.1762	0.1856	5.33

It is observed that the evolution of the value of R_s does not follow a coherent pattern between the five cells. Cell 1 recorded a decrease of approximately 12.64% in ohmic resistance after use, a phenomenon that can be attributed to physical adjustments of the contacts or reconfiguration of the ion path following the operating cycles. In contrast, cell 2 showed an increase in this parameter by 5.45%, and cell 4 a variation of 2.82%, which may signal a slight mechanical degradation or changes in internal conductivity. Cell 5 recorded a decrease of 3.56%, while cell 3 is the only one that remained almost constant, with a variation of 0.05%, considered insignificant from a practical point of view.

Overall, these results suggest that changes in ohmic resistance are not relevant for the assessment of functional degradation, being considerably influenced by local factors and contact variations. At the same time, the lack of a uniform trend limits the direct usefulness of this parameter in the comparative diagnosis of cells.

The R_{ct} parameter, which reflects the contact conditions between the electrode and the electrolyte in electrochemical processes, showed a clear and systematic evolution in all five cases. There were increases in the R_{ct} value after use for all cells, with percentage deviations between +4.41% (cell 1) and +9.22% (cell 3). This trend confirms the presence of degradation processes at the electrode-electrolyte interface, such as thickening of the passive layer (SEI), accumulation of reaction products, or reduction of the electrochemically available active surface.

The fact that all cells show such growth, consistently, indicates a degradation specific to use in real applications.

The results obtained by the EIS analysis provide a coherent basis for the comparative assessment of the health status of the cells used, allowing the identification of those with advanced degradation and providing support in decisions to reconfigure or withdraw modules from use.

Chapter 9

Alternative modeling and simulation of hybrid operation of residential PV system

In continuation of the analysis of the existing residential photovoltaic system, this chapter proposes an alternative variant of extension of the architecture by integrating a DC-coupled configuration. If in the previous Chapter a hybridization solution based on a Victron MultiPlus II inverter, connected to the AC-coupled side, was analyzed, this chapter explores the possibility of using only the Fronius Primo 8.2-1 inverter already installed, by adapting the system to allow automatic switching between photovoltaic strings and a Li-ion battery pack.

Modeling and simulation are performed in the MATLAB/ Simulink environment in order to evaluate the energy behavior of the proposed configuration in day-night operation. The advantages and limitations of this solution are highlighted from the perspective of electrical compatibility with the existing inverter, as well as from the point of view of automatic control of the sources.

9.1. Objective of the simulation

The initial configuration of the analyzed battery (19s3p), was reconfigured in a 28s2p structure to comply with the voltage requirements imposed by the proposed DC-coupled architecture. This change allows compatibility with the operating range of the Fronius Primo 8.2-1 inverter MPPTs and ensures continuity of power supply at night. The reconfiguration provides an adequate voltage rating and sufficient capacity to sustain a constant flow of energy in the absence of photovoltaic generation.

Based on this structure, the objective of the simulation is to validate the operation of a hybrid photovoltaic system in DC-coupled configuration, in which the photovoltaic sources and the Li-ion battery are directly connected to the two MPPT inputs of the inverter. The model follows the automatic switching between the PV2 string and the LG Chem 28s2p battery pack, depending on the variation of solar irradiation, simulated by a day/night logic signal.

9.2. Modeled System Configuration

In order to simulate and evaluate the performance of the analyzed system, we defined a representative configuration, integrating the two distinct photovoltaic strings, the Li-ion battery pack and the inverter with two independent MPPT trackers, as follows:

– PV1 string consisting of 12 photovoltaic panels Sharp NU-JD540W: V_{mpp} = 499,7V; I_{mmp} = 12,97A;

– PV2 string consisting of 8 photovoltaic panels Longi LR5-66HTH-525M: V_{mmp} = 320,5V; I_{mmp} = 13,11A;

– LG Chem battery configured 28s2p: V_{nom} = 100,8V; V_{max} = 117,6V; C_{nom} = 116,8Ah;

– invertor Fronius Primo 8.2-1: two independent MPPTs, working interval 80 – 450V, maximum current 18A/ MPPT.

This configuration has been selected to ensure technical compatibility between components, as well as to allow detailed analysis of the interactions between photovoltaic sources, the storage system and the grid, under various operating conditions.

9.3. Modeling and simulation of the hybrid system in Matlab/ Simulink

The modeling was performed in the Matlab/ Simulink environment, using logic blocks and signal sources, and the block diagram is shown in Figure 9.1:

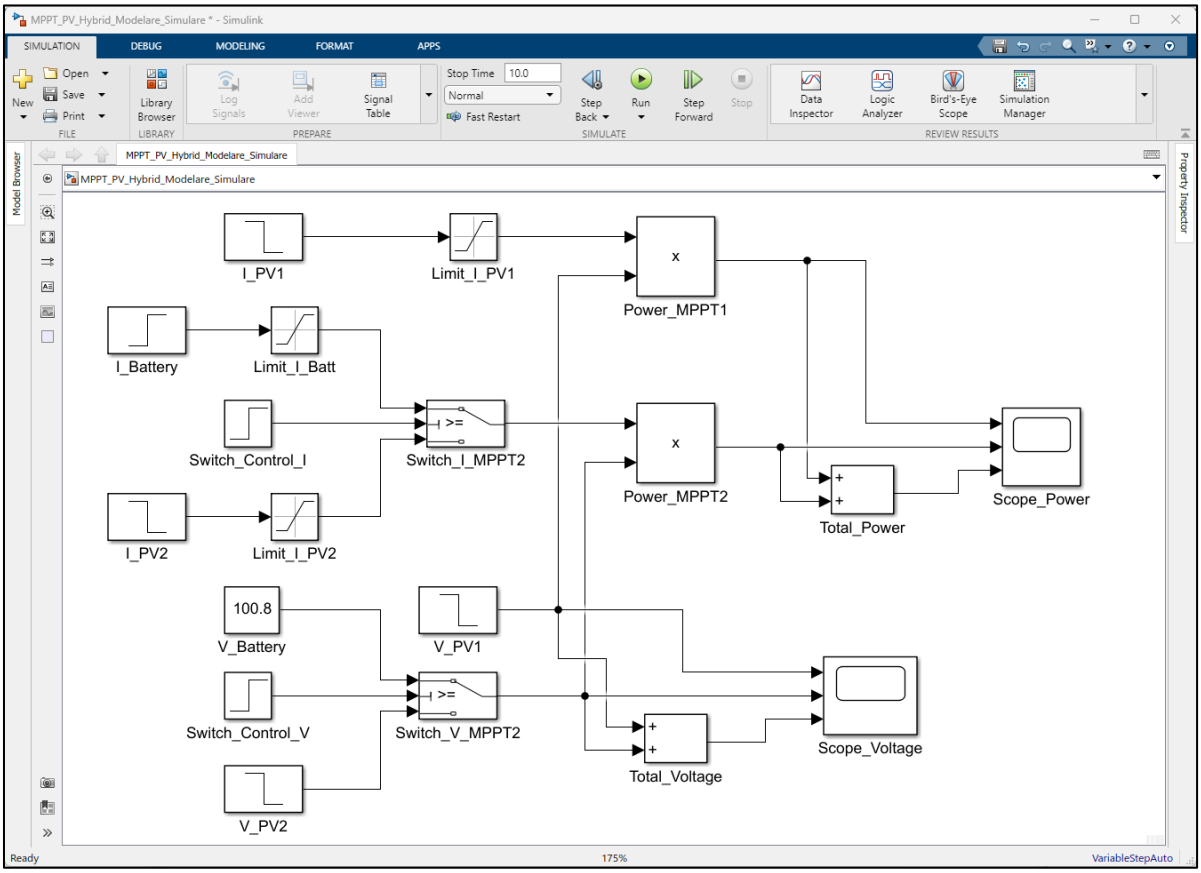


Figure 9.1 Simulink Model Block Diagram

➢ *Modeling of photovoltaic panels*

For each photovoltaic string, *Step blocks* (*I_PV1, I_PV2*) configured to reproduce the characteristic current and voltage values at the maximum power point for the two sets of panels were used. These signals are limited to 18A through *Saturation blocks* (*Limit_I_PV1, Limit_I_PV2*) to match the technical specifications of the Fronius Primo 8.2-1 inverter MPPTs.

The voltage values are combined with the current values in *Product* blocks (*Power_MPPT1, Power_MPPT2*), resulting in the power obtained on each string.

- *Battery modelling*

The LG Chem battery pack configured 28s2p is represented by a *Step* (*I_Battery*) block and a *Constant* block (*V_Battery*) corresponding to the maximum available current and rated voltage. They are used in switching with the second MPPT of the inverter, ensuring its supply under conditions of low irradiation (night). Also in this case, the current is limited to protect the MPPT with the help of a *Saturation* block (*Limit_I_Batt*).

- *Logica de comutare automată*

The switching between the photovoltaic sources and the battery is carried out with the help of two *Switch blocks* (*Switch_I_MPPT2, Switch_V_MPPT2*), controlled by logic signals such as *Step* (*Switch__Control_I, Switch_Control_V*), with a t = 5s transition, astfel:

– before t = 5s (day): the output is 1 → PV2 activation
– after t = 5s (night): the output is 0 → battery activation

Thus, these signals simulate the day-night transition and activate the connection of the battery to the MPPT2 during the period without solar production. The logic also involves comparators that evaluate control signals to selectively switch between PV2 and battery.

- *Power calculation and display of results*

The power generated on each MPPT is calculated using *Product blocks* (*Power_MPPT1, Power_MPPT2*), and their sum is represented by a block of type *Sum* (*Total_Power*). Power and voltage values are monitored in real time by *Scope blocks* (*Scope_Power, Scope_Voltage*), allowing dynamic analysis of operating regimes and transitions imposed by switching logic.

9.4. Interpretation of simulation results

The results obtained from the simulation indicate the electrical voltage and power curves. They reflect the realistic behavior of the hybrid photovoltaic system in day/night operation. In the initial range (t < 5s), both MPPTs are powered exclusively by the PV1 and PV2 strings, ensuring the conversion of solar energy into available active power at the inverter output.

After the moment t = 5s, the logic control causes the PV2 source to be switched with the LG Chem battery. The MPPT2 continues to provide power, but this time from the accumulated stock in the battery. This transition can be seen directly in the Scope_Power signal where power remains active after sunset, unlike conventional on-grid systems that cease operation in the absence of solar irradiation.

The following analysis examines the behaviour of the hybrid PV system with automatic switching between the PV2 string and the LG Chem 28s2p battery pack:

- *Behavior in day mode (0 – 5s):*

By the time t = 5s, the photovoltaic sources are active, the irradiation is maximum, and both MPPTs are powered by the PV1 and PV2 strings. During this period:

– the power on MPPT1 is constant around 6480Wp, corresponding to the current of 12.97A and the voltage of 499.7V;

– the power on MPPT2 is about 4200Wp, resulting from the 13.11A and 320.5V of the PV2 string;

– total power reaches a maximum of 10680Wp (according to Scope_Power);

– the total input voltage is approximately 820.2V (499.7V + 320.5V), confirming the smooth operation in the DC-coupled configuration.

➢ *Behavior in night mode (after 5s):*

After the moment t = 5s, the *day/night switching signal* causes the PV2 string to be deactivated and switched to battery:

– the power on MPPT1 drops to 0W, confirming the absence of irradiation and implicitly stopping the production of the PV1 string;

– the MPPT2 now receives current and voltage from the battery (100.8V and 18A), and the power generated drops to about 1800W;

– total system power becomes 1800W, exclusively reflecting the battery input;

– the total voltage is now 100.8V, equal to the value of the battery voltage, as PV1 and PV2 are non-functional in the absence of irradiation.

➢ *Validation of system behavior:*

The simulation confirms:

– correct operation of automatic switching depending on irradiation;

– maintaining battery power at night with adequate voltage and power for light loads applicable to the inverter output;

9.5. Conclusions

Modeling in Simulink demonstrates the possibility of extending an existing residential PV system by integrating a secondary energy source (battery) into a DC-coupled architecture, without modifying the already installed on-grid inverter. The simulation of the automatic switching between the photovoltaic strings and the battery according to the day/night cycle allows to highlight the advantages of such a configuration in terms of continuity of power and efficient use of stored energy.

From a theoretical and simulation point of view, the idea of replacing a PV string with an equivalent source of direct current (battery with compatible voltage) is valid. In practice, however:

– it is necessary to add a BMS that accurately manages the current and voltage supplied, but also with over-discharge protection and thermal monitoring;

– compatibility with the inverter's MPPT algorithms must be validated;

– the inverter should not interpret the constant voltage of the battery as an anomaly.

Therefore, the approach can be implemented in real systems, but requires rigorous compatibility and electrical safety checks.

Chapter 10

Comparative analysis of PV system performance with and without energy storage: energy and economic impact

This chapter aims at the comparative analysis of the performance of the photovoltaic system in the two distinct configurations: before and after the integration of the energy storage system. The study focuses on the impact of adding the battery on key relevant energy and economic indicators, such as self-consumption, the level of energy independence, the efficiency of solar energy use, as well as the interaction with the electricity grid. The aim is to highlight the advantages, limitations and technical-economic potential of hybridization of the photovoltaic system through local storage.

The evaluation is based on real operating data for two distinct periods: 01.06.2023 – 31.05.2024, in classic on-grid configuration (without storage), and the second, 13.06.2024 – 12.06.2025, in hybrid configuration, with second-life LG Chem batteries integrated into the system by Victron Energy equipment in AC coupling with the Fronius Primo 8.2-1 inverter.

10.1. Energetic impact

10.1.1. Energy analysis of the photovoltaic system in on-grid configuration (basic configuration)

The evolution of the electricity produced by the photovoltaic system in this configuration is presented, over a full year (1.06.2023 – 31.05.2024). The data presented were obtained with the help of the *Solar Web* application. The energy generated was structured in two components: energy delivered to the grid, which represents the surplus energy not used locally and injected into the national system, and direct consumption, i.e. energy used in real time by the consumer (Table 10.1).

Table 10.1 Distribution of energy produced by the PV system in the period 1.06.2023 –31.05.2024

Period	To grid (kWh)	Direct consumption (kWh)	Total (kWh)
01.06.2023 – 31.05.2024	6529.97	1729.78	8260.82

The electricity consumption, broken down by source of origin (energy supplied from the public grid and energy used directly from local photovoltaic production), is presented in Table 10.2.

Table 10.2 Energy consumed between 1.06.2023 – 31.05.20214

Period	From grid (kWh)	From solar energy (kWh)	Total (kWh)
01.06.2023 – 30.06.2023	2065.59	1729.78	3795.37

10.1.2. Energy analysis of the photovoltaic system in hybrid configuration (with the integration of energy storage)

Between 13.06.2024 – 12.06.2025, the system was expanded by integrating a second-life LG Chem battery pack, using Victron Energy controllers and maintaining the Fronius inverter for solar conversion. In this new architecture, excess solar energy was redirected to the batteries instead of being lost or blocked by surges.

The Victron control system (Cerbo GX) intelligently managed energy flows, allowing surplus production to be stored and then used to cover residential consumption or for controlled grid injection. When solar production is insufficient, the necessary energy is taken from the public grid.

In order to further analyze the energy behavior of the photovoltaic system after battery integration, it was evaluated how the solar energy produced is directed to different consumption or storage destinations. Table 10.3 shows the distribution of the energy generated by the photovoltaic system between 13.06.2024 – 12.06.2025, differentiated into three main flows: the energy injected into the grid, the energy used to charge the battery and the energy consumed directly (energy used in real time by the consumer). The data was obtained using the *Victron Energy Vrm application*.

Table 10.3 Distribution of energy produced by the PV system between 13.06.2024 – 12.06.2025

Period	To grid (kWh)	To battery (kWh)	Direct consumption (kWh)	Total (kWh)
13.06.2024 – 12.06.2025	6264.29	2968.35	2307.26	11539.93

The amounts of energy consumed from each source are summarised in Table 10.4.

Table 10.4 Monthly amounts of energy consumed from each source

Period	From grid (kWh)	From battery (kWh)	From solar energy (kWh)	Total (kWh)
13.06.2024 – 12.06.2025	393.45	2186.45	2307.26	4889.18

10.1.3. Comparative analysis

The comparative analysis of the operation of the photovoltaic system in on-grid mode and later in hybrid configuration highlights a significant improvement in energy efficiency and energy autonomy.

Between 01.06.2023 and 31.05.2024, the system operated exclusively on-grid. The annual energy produced was 8260.82kWh (Table 10.1). The energy used in real time by consumers was 1729.78kWh, a relatively low consumption (around 18–22% monthly), the rest being injected into the grid (Figure 10.8). The total annual consumption was 3795.37kWh, of which a large part was provided by energy imported from the grid (Figure 10.9), 2065.59kWh (Table 10.2.).

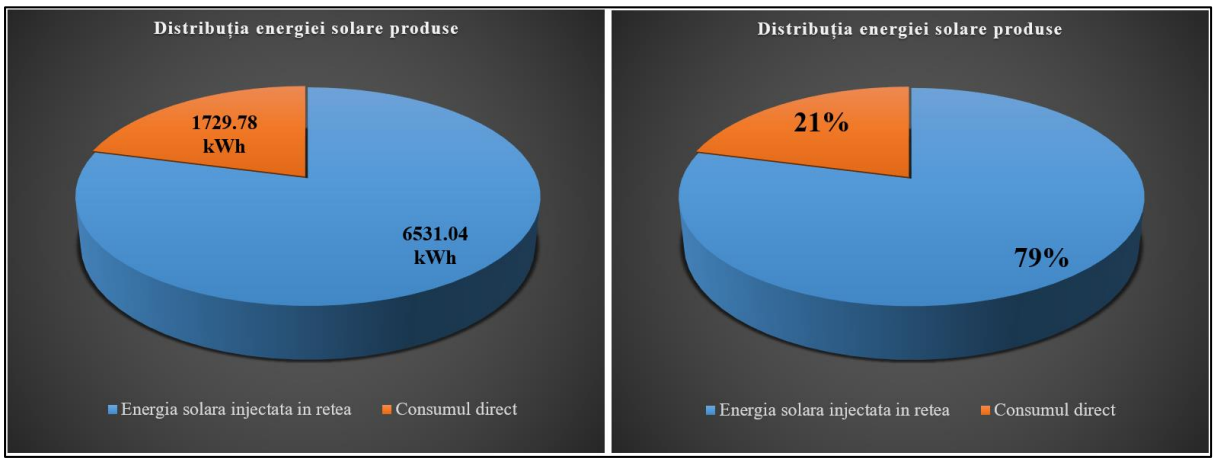


Figure 10.8 Distribution of solar energy produced in the on-grid system

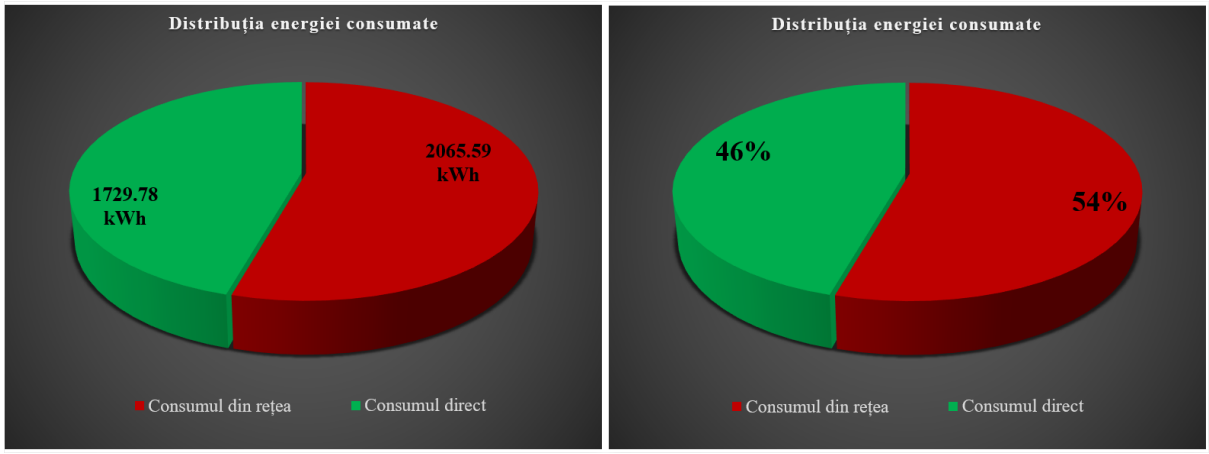


Figure 10.9 Distribution of energy consumed with on-grid system

In the absence of a storage system, the grid provided 54% of the total annual consumption, reflecting a high dependence on the distribution grid and an inefficient use of the solar energy produced.

After integrating the LG Chem second-life battery and expanding the production capacity, the system produced a larger amount of energy, 11539.93kWh (Table 10.3), and ensured a more efficient use of it: direct consumption increased to 2307.26kWh, the energy storage unit stored a total amount of 2968.35kWh, and 6264.29kWh was injected into the grid

(Figure 10.10). According to Table 10.4, the total annual consumption was 4889.18kWh (Figure 10.11), as follows:

- 2307,26kWh from solar energy;
- 2186,45kWh from the storage system;
- 393,45kWh from grid.

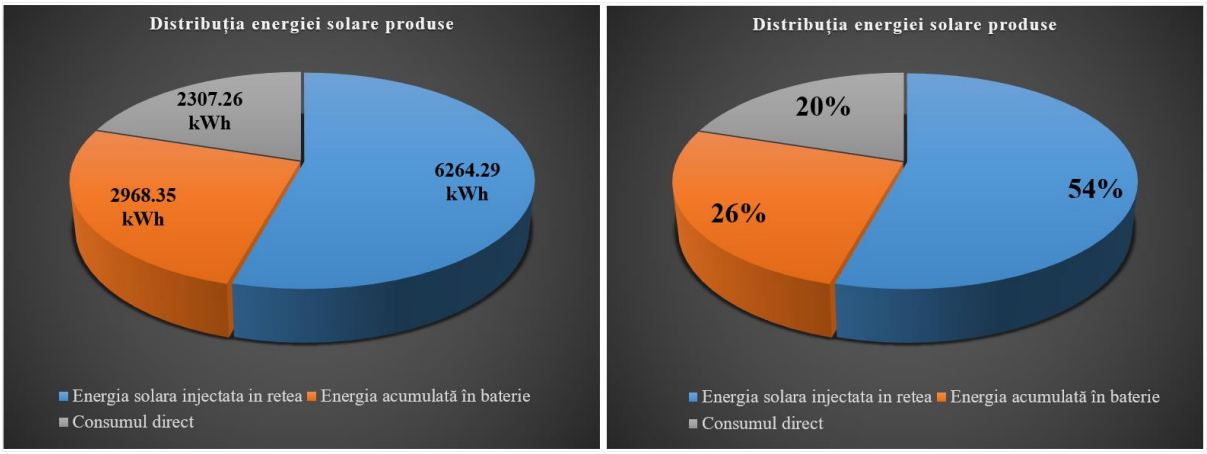


Figure 10.10 Distribution of solar energy produced in hybrid configuration

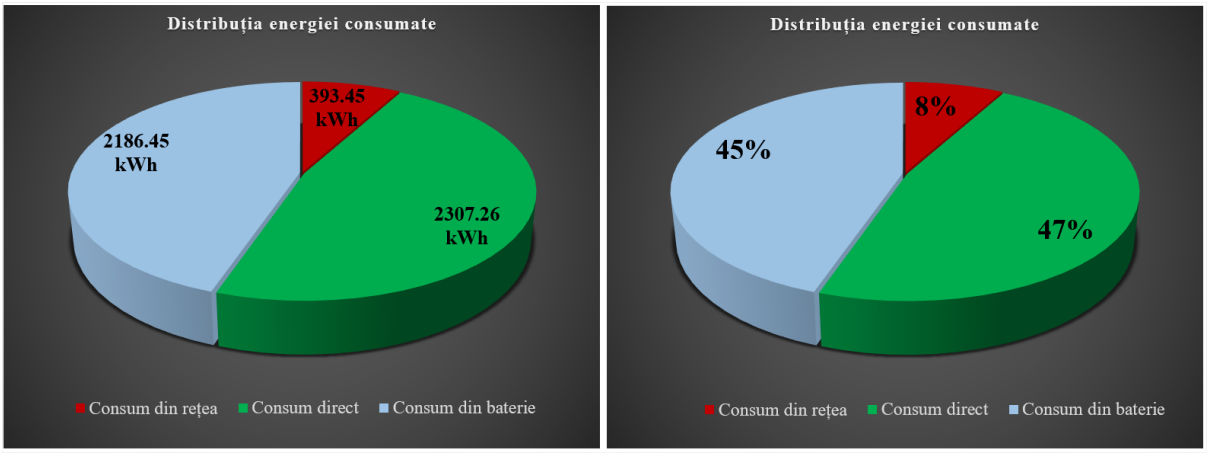


Figure 10.11 Distribution of energy consumed in hybrid configuration

It can be seen that the energy consumed from the grid has been considerably reduced, from 54% to 8%. This change has led to a considerable decrease in dependence on the electricity grid and has allowed a more efficient use of locally available photovoltaic energy, by reducing the losses associated with injection and limiting the effects of surges.

The data presented illustrate the performance differences between the two configurations and based on them it can be concluded that the integration of the second-life battery has led to: an increase in the self-consumption rate, a reduction in the energy lost by disconnecting the inverter, a decrease in the import of energy from the grid and an increase in the energy value of the system. The system thus becomes more autonomous, more efficient in the use of available solar energy and more stable in relation to the electricity grid. This performance is supported by the intelligent use of storage and the system's ability to dampen voltage fluctuations by absorbing surplus into the batteries.

10.2. Economic impact

10.2.1. Economic analysis of the photovoltaic system in on-grid configuration (basic configuration)

For the period of operation without storage (01.06.2023 – 31.05.2024), the energy supplier recorded a total of 6297.59kWh of which 4232.00kWh were directly remunerated, and 2065.59kWh were recorded as quantitative compensation for grid consumption (Table 10.5). According to the *Solar Web* monitoring system, 6529.97kWh of solar energy was injected into the grid, and the difference between this value and the one recorded by the supplier (232.38kWh) is considered a loss when injected into the grid.

Table 10.5 Energy produced in relation to the energy supplier (on-grid system)

Period	Compensate 1:1 (kWh)	Consumption direct (kWh)	To grid, according to the energy supplier (kWh)
01.06.2023 – 31.05.2024	2065.59	1729.78	4232.00

The associated prices per kWh for each category of energy used are as follows:

– 4232.00kWh (energy injected into the grid) are remunerated at an average price of 0.5613 lei/kWh;

– 2065.59kWh (energy consumed from the grid and compensated 1:1) correspond to the price of 0.80 lei/kWh [45], but only 0.5613 lei/kWh are reimbursed by the supplier, the rest up to 0.80 lei/kWh cover the transmission tariffs/tariff limit of the distribution company, according to Table 10.6;

– 1729.78kWh (direct consumption from solar energy), are taken into account with the price of 0.80 lei/kWh, as they would have been purchased directly from the energy supplier [45].

Table 10.6 Difference in payment (lei/kWh) to the supplier (01.06.2023 – 31.05.2024)

Purchase price from the grid (lei/ kWh)	Average price offered by the supplier (lei/ kWh)	Transport tariff/ tariff plafonare (lei/ kWh)
0.80	0.5613	0.2387

Table 10.7 shows the amounts for each category of electricity.

Table 10.7 Amounts related to each category of electricity (on-grid system)

Energy category	Quantity (kWh)	Price (lei/ kWh)	Total (lei)
Compensate 1:1 (kWh)	2065.59	0.5613	1159.42
Transport tariff / tariff limit for compensation 1:1 (kWh)	2065.59	-0.2387	-493.06
Direct consumption (kWh)	1729.78	0.80	1383.82
To the grid according to the energy supplier (kWh)	4232.00	0.5613	2375.42

The balance sheet for the analyzed period (12 months) indicates a profit of 4425.60 lei (ratio 10.1).

$$1159.42lei - 493.06lei + 1383.82lei + 2375.42lei = 4425.60\ lei \quad (10.1)$$

10.2.2. Economic analysis of the photovoltaic system in hybrid configuration (with the integration of energy storage)

For the period of operation in hybrid configuration (13.06.2024 – 12.06.2025), the energy supplier recorded a total of 6545.45kWh of which 6152.00kWh were directly remunerated, and 393.45kWh were recorded as quantitative compensation for the consumption in the network (Table 10.8).

Table 10.8 Energy produced in relation to the energy supplier (hybrid system)

Period	Compensate 1:1 (kWh)	Direct consumption (kWh)	From battery (kWh)	To grid, according to the energy supplier (kWh)
13.06.2024 – 12.06.2025	393.45	2307.26	2186.45	6152.00

According to the Cerbo GX monitoring system, 7046.19kWh of solar energy was injected into the grid, of which:

– 6264.29kWh were injected into the grid directly from solar production;

– 781.90kWh were injected from the storage system;

The difference between the value measured by the Cerbo GX monitoring system and the value recorded by the supplier (500.74kWh) is considered loss when injected into the grid and/or by inverter-storage system conversion and vice versa.

The prices per kWh associated with each category of energy used are detailed as:

– the energy purchased from the grid, 393.45kWh, is associated with two tariffs [45]: the quantity of 155.07kWh in December 2024 was purchased at the price of 0.80 lei/kWh and the quantity of 238.28kWh corresponding to the other 11 months was purchased at the price of 0.68 lei/kWh. For both tariffs, only 0.5775 lei/kW are reimbursed by the supplier, the rest up to 0.80 lei/kWh, respectively 0.68 lei/kWh, covers the transmission tariffs/ tariff capping of the distribution company, according to Table 10.9.

– 2307.26 kWh (direct consumption from solar energy), are taken into account with the price of 1.30 lei/kWh, as they would have been purchased directly from the energy supplier;

– 2186.45kWh (from battery consumption), are also taken into account with the price of 1.30 lei/kWh, as they would have been purchased directly from the energy supplier [45];

– 6152.00kWh are remunerated with an average price of 0.5775 lei/kWh.

Table 10.9 Difference in payment (lei/kWh) to the supplier (13.06.2024 – 12.06.2025)

Purchase price from grid (lei/ kWh)	Average price offered by the supplier (lei/ kWh)	Transport tariff/ tariff limit (lei/ kWh)
0.80	0.5775	0.2225
0.68	0.5775	0.1025

Table 10.10 shows the amounts for each category of electricity.

Table 10.10 Amounts related to each category of electricity (hybrid system)

Energy category	Quantity (kWh)	Price (lei/ kWh)	Total (lei)
Compensate 1:1 (kWh)	155.07	0.5775	89.55
	238.28	0.5775	137.61
Transport tariff / tariff limit for compensation 1:1 (kWh)	155.07	-0.2225	-34.50
	238.28	-0.1025	-24.42
Direct consumption (kWh)	2307.26	1.30	2999.44
From battery consumption (kWh)	2186.45	1.30	2842.38
To grid according to the energy supplier (kWh)	6152.00	0.5775	3552.78

The balance sheet for the analyzed period (12 months) indicates a profit of 9562.84 lei.

$$89.55lei + 137.61lei - 34.50lei - 24.42lei + 2999.44lei + 2842.38lei + 3552.78lei = 9562.84\ lei \quad (10.2)$$

10.3. Amortization of the investment

10.3.1. Return on investment for on-grid photovoltaic system

In order to evaluate the profitability of the photovoltaic system in on-grid configuration, the total purchase cost of the components was used, means 30995.00 lei. Based on the annual operating data, the system generated a profit composed of the value of the energy consumed directly and the energy obtained through the injection into the network, totaling approximately 4425.60 lei/year.

Thus, the payback period of the investment (amortization) can be estimated by the ratio between the initial investment and the annual profit, resulting in:

$$Payback\ period = \frac{30995.00\ lei}{4425.60\ {}^{lei}/_{year}} = 7\ years \quad (10.3)$$

10.3.2. Amortization of the investment for the hybridized PV system

Following the transformation of the photovoltaic system from an on-grid configuration to a hybridized system, a detailed economic analysis of the financial performance was carried out for the period 13.06.2024 – 12.06.2025. This system was composed of the initial photovoltaic infrastructure, to which storage equipment (LG Chem second-life batteries) and Victron devices were added for their integration. The cost of the on-grid system was 30995.00 lei, and the additional cost for the storage and hybridization component was 19545.75 lei. Thus, the total investment for the hybridized photovoltaic system amounts to 50540.75 lei.

Relating the total value of the benefits (9562.84 lei/year) to the cost of the investment (50540.75 lei), the result is an estimated amortization period of approximately 5.28 years under the current conditions. This performance is due to the system's ability to store surplus PV and reduce grid surge losses, which previously affected the efficiency of the on-grid system.

$$Payback\ period = \frac{30995{,}00lei + 19545{,}75\ lei}{9562{,}84\ {}^{lei}/_{year}} = 5{,}28\ years \qquad (10.4)$$

As in the case of the on-grid system, the estimate made assumes maintaining the performance of the photovoltaic panels and the inverter over time, in the absence of significant degradation, as well as maintaining energy tariffs at a stable level. However, under real operating conditions, the payback period may vary depending on changes in the consumption profile, fluctuations in the level of solar irradiation, the evolution of regulated tariffs and the reliability of the system components.

10.4. Conclusions

The comparative analysis of the two configurations of the photovoltaic system (on-grid and hybridized with storage system) highlights a significant improvement in economic performance with the integration of batteries and auxiliary energy management equipment. The on-grid system generated an annual profit of approximately 4425.60 lei, leading to an estimated amortization period of 7 years, while the hybridized system, with an additional investment in storage and control components, recorded an annual profit of 9562.84 lei, reducing the amortization period to approximately 5.28 years.

These results highlight the economic potential of the hybridization of residential PV systems, especially in the context of grids with voltage fluctuations or injection restrictions. Increasing the degree of self-consumption and capitalizing on the photovoltaic surplus through storage directly contributes to optimizing the return on investment.

However, it is important to stress that these estimates are based on idealised assumptions, such as the maintenance of the technical performance of the equipment without significant degradation and the stability of energy tariffs. Under real-world operating conditions, the actual payback time may be influenced by variations in user consumption, local climate changes (affecting solar irradiation), regulated tariff adjustments, and the reliability of the components used in the system. Therefore, for a robust and sustainable estimate, it is recommended to regularly monitor the energy and financial performance of the system in operation.

Chapter 11

Conclusions

The evolution of on-grid systems in Romania is characterized by significant growth, supported by financial stability, government support and environmental considerations. The concept of prosumer has gained importance, with their number visibly increasing as a result of legislative changes and support programs. However, this expansion puts pressure on the national low-voltage grid, generating voltage fluctuations and possible disturbances. To mitigate these effects, innovative solutions are needed, including the use of advanced technologies such as energy storage systems and hybrid configurations. Current developments highlight the need for a balanced approach, taking into account environmental benefits, economic implications and technical requirements. The trend points to continued growth in the adoption of on-grid systems, with an increasing focus on grid compatibility and increasing system resilience.

The present paper aimed at integrating a second-life battery from an electric vehicle into a residential photovoltaic system and investigating the real possibilities of its expansion, optimization and hybridization. During the research, essential steps were taken, from the comparative analysis of the available storage technologies and the selection of the battery pack, to the experimental testing of the performance of the selected cells and the validation of the proposed hybrid configuration.

The study highlighted that second-life lithium-ion batteries, especially NMC batteries from electric vehicles, can be a viable alternative for stationary energy storage applications. Through static testing, hybrid pulse power characterization test and electrochemical impedance spectroscopy of the selected LG Chem cells, it was possible to characterize their condition before and after integration into the photovoltaic system, obtaining relevant data on capacity, internal resistance and degradation over time. The experimental results showed a moderate loss of active capacity, but without compromising the operation of the system within acceptable functional parameters.

The integration of the battery in an AC-coupled configuration has allowed to increase the level of self-consumption and reduce the losses associated with uncontrolled injection into the grid, especially in periods of low consumption and high solar production. Simulations performed in MATLAB/ Simulink also confirmed the functionality and efficiency of the proposed alternative hybrid architecture.

Energy and economic analysis has shown that upgrading the system by adding a storage component leads to a significant improvement in overall performance, leading to a payback period comparable or even shorter than in the classic on-grid configuration. The additional investment costs for battery integration are compensated by capitalizing on surplus energy and increasing energy independence.

The comparative analysis of energy flows from June 13, 2024 to June 12, 2025 highlights the performance of the hybrid photovoltaic system in real operating conditions, with significant seasonal variations. Battery integration has had a key impact on the1

– reducing dependence on the grid, especially in months with high solar production;
– maximizing self-consumption, by absorbing solar surplus and covering consumption outside irradiation hours;
– limiting grid injection outside summer periods due to storage capacity.

According to statistics provided by Fronius *Solar.web* application, the photovoltaic system produced, over the entire operating period, 30.54 MWh, equivalent to the emission of 16.18 tons of CO_2 into the atmosphere. This emissions savings are equivalent to planting around 415 trees that would have absorbed the same amount of CO_2 over their lifetime, or driving around 64928 km in a combustion car, which would have generated similar emissions (Figure 11.1). These indicators illustrate the direct contribution of the PV system to reducing its environmental impact by replacing some of the energy from conventional sources with locally produced renewable energy.

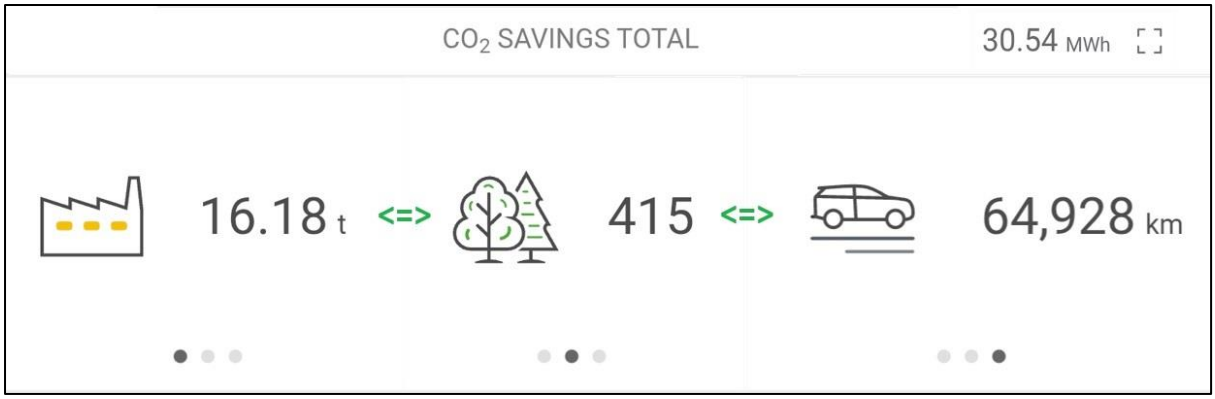


Figure 11.1 Contribution of the photovoltaic system to reducing environmental impact

Therefore, this paper contributes to substantiating the decision to reuse second-life batteries in the context of the energy transition and the promotion of sustainability. An integrated perspective on the opportunities and limitations of this approach is provided, supported by concrete experimental results and relevant technical-economic simulations.

11.1. Results obtained

As a result of the research carried out in this work, relevant results were obtained that confirm the feasibility and potential of integrating second-life batteries into on-grid photovoltaic systems, contributing to the development of sustainable energy storage solutions.

The analysis of the literature and existing technologies made it possible to identify the constructive and functional characteristics of the different types of batteries used in the field of electric vehicles, with a focus on the NMC technology used by LG Chem. On this basis, a battery pack from a Hyundai Kona Electric 64kWh electric vehicle was selected and purchased, which was subsequently disassembled and configured for integration into a storage system stationary.

The experimental testing, carried out in the "Battery Testing" laboratory, comprised three major stages:

– static capacity test – used to determine the actual capacity of cells before and after use;

– HPPC test – used to characterize internal resistance and available power depending on the state of charge;

– electrochemical impedance spectroscopy (EIS) – intended to evaluate internal electrochemical parameters and identify possible structural changes in cells.

The comparison of the results obtained before and after integration into the PV system showed a moderate decrease in capacity and a slight increase in internal resistance, without affecting the overall functionality of the battery pack in the stationary application. This result reflects a slow and uniform degradation, characteristic of a stable electrochemical behavior under real operating conditions.

The integration of the second-life battery in an AC-coupled configuration, together with an existing Fronius Primo 8.2-1 system, allowed the energy flow to be optimised by reducing the surplus injected into the grid and increasing the use of locally produced energy. Thus, the functionality of the proposed architecture is confirmed and its potential to improve the energy parameters of the home is highlighted. The simulation performed in MATLAB/ Simulink could be considered an alternative to the experimentally analyzed hybridized configuration, by testing the concept of direct connection of the battery to the MPPT input of the on-grid inverter (DC-coupled architecture). The modeling highlights the possibility of expanding an existing residential PV system by integrating a secondary energy source without modifying the inverter already installed, as well as the benefits of automatic switching between PV strings and battery depending on the day/night cycle, in order to ensure continuity of power supply and optimal use of stored energy.

The energy and economic analysis has shown that the integration of the second-life storage solution reduces dependence on the grid, increases the degree of self-consumption and can ensure a competitive return on investment compared to the classic on-grid configuration. The expansion of the photovoltaic field by adding 8 more PV modules has led to a significant increase in production, ensuring a greater coverage of consumption from own sources. At the same time, the comfort of the residential environment was improved by purchasing additional household appliances, powered mainly by locally generated energy, which allowed the diversification of daily activities without increasing recurring electricity costs. Thus, the combination of increased production with fuel consumption optimisation has strengthened the technical and economic performance of the hybrid configuration, while also contributing to increasing user comfort.

Therefore, the main conclusions and results are as follows:

– second-life batteries are a viable technical solution for on-grid photovoltaic systems, maintaining adequate performance for energy storage in the medium and long term;

– AC-coupled configuration ensures efficient and flexible integration of reused batteries, facilitating optimal energy management between production, storage and consumption, with a positive impact on the power grid;

– the test methods applied have demonstrated the ability to accurately diagnose battery health, being useful for performance monitoring and lifecycle management decision-making;

– the integration of second-life batteries contributes both to reducing the costs of storage systems and to reducing the environmental impact of used batteries, supporting the sustainable energy transition;

– for the large-scale deployment of these solutions, it is necessary to develop clear standards on battery reuse, as well as to implement effective monitoring and maintenance strategies.

The results obtained validate the hypothesis that the integration of second-life batteries in residential photovoltaic systems is a feasible solution, with technical and economic benefits, contributing to the implementation of sustainable energy production and management strategies.

11.2. Original contribution

This doctoral thesis presents original contributions to the field of integration of second-life batteries in on-grid photovoltaic systems, through a combined, theoretical and experimental applicative approach. The main contributions include:

– selection and configuration of a second-life battery pack from a Hyundai Kona Electric 64kWh electric vehicle, using traceability, reliability and compatibility criteria, according to the ISO 2859-1 sampling methodology, in order to adapt to a stationary AC-coupled application;

– the development and implementation of an experimental test plan for second-life cells, which combines the static capacitance test, the HPPC test and electrochemical impedance spectroscopy (EIS), allowing a characterization of electrochemical performance both before and after use in the photovoltaic system;

– determination of the optimal loading and discharging thresholds for the LG Chem cells in the analyzed package, in order to maximize the service life in the stationary application and establish the configuration parameters of the JK-PB2A16S-20P BMS;

– evaluation of the impact of the large number of prosumers belonging to on-grid photovoltaic systems on the low voltage grid and development of an evaluation model that analyzes the impact of the integration of second-life batteries on the increase of self-consumption, the reduction of energy taken from the electricity grid during peak periods and the general stability and reliability of the photovoltaic system;

– the design and practical implementation of an AC-coupled technical configuration adapted to the particularities of second-life batteries, which optimizes the management of energy flows between photovoltaic panels, household consumers, the storage system, and the public electricity grid;

– realization, in the MATLAB/Simulink environment, of a simulation that can be considered an alternative to the experimentally analyzed hybridized configuration, with the objective of testing the concept of direct connection of the battery to the MPPT input of the on-grid inverter, in a DC-coupled architecture. The modeling obtained highlights the possibility of extending an existing residential photovoltaic system by integrating a secondary energy source, without modifying the inverter already installed;

– conducting a detailed comparative analysis, both from an energy and economic perspective, between the basic on-grid configuration and the hybrid configuration with second-life storage, highlighting its positive impact on system performance and payback period.

Overall, the contributions of this paper provide a methodological and applicative framework for assessing the technical, economic and ecological feasibility of reusing second-life batteries in residential photovoltaic systems, with potential for replication in similar projects, supporting the transition to sustainable and flexible energy solutions.

11.3. Prospects for further development

Considering the results obtained from the integration of a second-life battery in an on-grid residential photovoltaic system, the future research directions can be oriented both towards deepening the technical aspects and extending the practical applicability of the proposed solution.

A first direction is to analyze the behavior of the system in the long term, by continuously monitoring the performance of the second-life battery under real operating conditions, in order to identify possible mechanisms of accelerated degradation or efficiency variations depending on the season. This approach would allow the validation of hypotheses formulated in laboratory tests and could help to improve lifespan prediction models.

Secondly, the expansion of the current configuration towards a fully autonomous (off-grid) or semi-autonomous (with intelligent grid support) architecture can be a normal step, involving the development of advanced energy management strategies based on artificial intelligence and real-time optimization algorithms.

At the same time, on an experimental level, it is recommended to investigate the behavior of other types of second-life cells to determine their adaptability to residential applications, as well as to compare various BMS technologies and communication protocols for the control and protection of the storage system.

In parallel, on the economic front, future research may include the analysis of business models for the reuse of second-life batteries, the study of legislative barriers and the identification of the necessary incentives for the widespread adoption of these solutions. The integration of these systems into smart grids and their participation in ancillary services markets could be a new opportunity for exploitation.

In conclusion, the further development of the research requires a multidisciplinary approach, including electrical engineering, materials science, economic analysis and energy policies, in order to strengthen the role of second-life batteries in the transition to a sustainable and flexible energy system.

Bibliografie

[1] I. T. Bello, H. Raza, A. T. Michael, M. Muneeswara, N. Tewari, W. Bingsen, Y. N. Cheung, Z. Choi, S. T. Boles, "Charging Ahead: The Evolution and Reliability of Nickel-Zinc Battery Solutions", EcoMat, vol. 7, no. 1, 2025, pp. 1-36. [Online]. doi: 10.1002/eom2.12505

[2] J. M. Abarro, J. N. Gavan, D. E. Loresca, M. A. Ortega, E. A. Esparcia, J. A. Paraggua, "A Tale of Nickel-Iron Batteries: Its Resurgence in the Age of Modern Batteries", Batteries, vol. 9, no. 383, 2023, pp. 1-44. [Online]. doi: 10.3390/batteries9070383

[3] H. Budde-Meiwes, B. Lunz, J. Muennix, S. Lehner, "A review of current automotive battery technology and future prospects", Article in Proceedings of the Institution of Mechanical Engineers Part D Journal of Automobile Engineering, 2013, pp. 760-776. [Online]. doi: 10.1177/0954407013485567

[4] M. T. von Srbik, "Advanced Lithium-ion Battery Modelling for Automotive Applications", Ph.D dissertation, Imperial College London, 2015, pp. 20-28. [Online]. https://spiral.imperial.ac.uk/server/api/core/bitstreams/9a64ea52-6aa8-4126-a7d3-1aff65c4c312/content

[5] https://batteryuniversity.com/article/bu-205-types-of-lithium-ion

[6] M. S. Houache, C. H. Yim, Z. Karkar, Y. A. Lebdeh, "On the Current and Future Outlook of Battery Chemistries for Electric Vehicles - Mini Review", Batteries, vol. 8, no. 70, 2022, pp. 1-19. [Online]. doi: 10.3390/batteries8070070

[7] S. Bauknecht, F. Wätzold, A. Schlösser, J. Kowal, "Comparing the Cold-Cranking Performance of Lead-Acid and Lithium Iron Phosphate Batteries at Temperatures below 00C", Batteries, vol. 9, no. 176, 2023, pp. 1-13. [Online]. doi: 10.3390/batteries9030176

[8] S. Clark, A. Latz, B. Horstmann, "A Review of Model-Based Design Tools for Metal-Air Batteries", Batteries, vol. 4, no. 5, 2018, pp. 1-26. [Online]. doi: 10.3390/batteries4010005

[9] T. R. B. Grandjean, J. Groenewald, A. McGordon, W. Widanage, J. Marco, "Accelerated Internal Resistance Measurements of Lithium-Ion Cells to Support Future End-of-Life Strategies for Electric Vehicles", Batteries, vol. 4, no. 49, 2018, pp. 1-17. [Online]. doi: 10.3390/batteries4040049

[10] A. Gailani, R. Mokidm, M. El-Dalahmeh, "Analysis of Lithium-ion Battery Cells Degradation Based on Different Manufacturers", 55th International Universities Power Engineering Conference (UPEC), 2020. [Online]. doi: 10.1109/UPEC49904.2020.9209759

[11] https://www.tesla.com/support/vehicle-warranty

[12] https://www.nissan.ro/gama/modele/leaf/garantie.html

[13] https://www.bmw.ro/ro/topics/offers-and-services/service-workshop/garantia-bmw.html

[14] https://www.volkswagen.ro/autovehicule-electrice-hibride/id-tehnologie/garantia-si-ingrijirea-bateriei

[15] https://www.hyundai-motor.ro/ro/model/kona-electric

[16] https://www.kia.ro/modele/ev6#;

[17]https://assets.rivian.com/2md5qhoeajym/4Gu8v9hXmik94CHAKis9mG/c6008f410cac191abd746bd60274bb22/r1t_r1s-new-vehicle-limited-warranty-guide-us-en-us-20241231.pdf

[18] L. Schwich, P. Sabarny, B. Friedrich, "Recycling Potential of Lithium-Sulfur Batteries – A First Concept Using Thermal and Hydrometallurgical Methods", Metals, vol. 10, no. 1513, 2020, pp. 1-19. [Online]. doi: 10.3390/met10111513

[19] A. Holzer, S. Windisch, C. Ponak, H. Raupenstrauch, "A Novel Pyrometallurgical Recycling Process for Lithium-Ion Batteries and Its Application to the Recycling of LCO and LFP", Metals, vol. 11, no. 149, 2021, pp. 1-22. [Online]. doi: 10.3390/met11010149

[20] L. Bruckner, J. Frank, T. Elwert, "Industrial Recycling of Lithium-Ion Batteries – A Critical Review of Metallurgical Process Routes", Metals, vol. 10, no. 1107, 2020, pp. 1-29. [Online]. doi: 10.3390/met10081107

[21] D. Werner, U. A. Peuker, T. Mutze, "Recycling Chain for Spent Lithium-Ion Batteries", Metals, vol. 10, no. 316, 2020, pp. 1-29. [Online]. doi: 10.3390/met10030316

[22] A. Patel, L. Lander, J. Ahuja, J. Bulman, J. K. H. Lum, J. O. D. Pople, A. Hales, Y. Patel, J. Edge, "Lithium-ion battery second life: pathways, challenges and outlook", Frontiers in Chemistry, vol. 12, 2024, pp. 1-21. [Online]. doi: 10.3389/fchem.2024.1358417

[23] E. Hossain, N. Sami, S. H. Sunny, "A Comprehensive Review on Second-Life Batteries: Current State, Manufacturing Considerations, Applications, Impacts, Barriers and Potential Solutions, Business Strategies and Policies", IEEE Access, vol. 7, 2019, pp. 73215-73252. [Online]. doi: 10.1109/ACCESS.2019.2917859

[24] T. Montes, M. Etxandi-Santolaya, J. Eichman, V. J. Ferreira, L. Trilla, C. Corchero, "Procedure for Assessing the Suitability of Battery Second Life Applications after EV First Life", Batteries, vol. 8, no. 122, 2022, pp. 1-19. [Online]. doi: 10.3390/batteries8090122

[25] J. Lacap, J. W. Park, L. Beslow, "Development and Demonstration of Microgrid System Utilizing Second-Life Electric Vehicle Batteries", Journal of Energy Storage, vol. 41, 102837, 2021, pp. 1-13. [Online]. doi: 10.1016/j.est.2021.102837

[26] S. Bobba, A. Podias, F. Di Persio, M. Messagie, P. Tecchio, A. Cusenza, U. Eynard, F. Mathieux, A. Pfrang, "Sustainability Assessment of Second Life Application of Automotive Bateries (SASLAB)", JRC Exploratory Research, Final technical report august 2018. [Online]. doi:10.2760/53624

[27] S. R. Das, P. K. Ray, A. K. Sahoo, K. K. Singh, G. Dhiman, A. Singh, "Artificial intelligence based grid connected inverters for power quality improvement in smart grid applications", Computers & Electrical Engineering, vol. 93, 2021, 107208. [Online]. doi: 10.1016/j.compeleceng.2021.107208

[28] M. Burlacu, V. Năvrăpescu, A. I. Chirilă, I. D. Deaconu, "Optimal reactive power management for microgrids based on photovoltaic inverters using sine-cosine algorithm", Revue Roumaine des Sciences Techniques - Serie Electrotechnique et Energetique, vol. 67, no. 2, 2022, pp. 117–122. [Online]. https://journal.iem.pub.ro/rrst-ee/article/view/189/155

[29] D. Beriber, A. Talha, A. Kouzou, A. Guichi, F. Boukhafaa, "Multilevel inverter for grid-connected photovoltaic systems", Revue Roumaine des Sciences Techniques - Serie Electrotechnique et Energetique, vol. 67, no. 2, 2022, pp. 105–110. [Online]. https://journal.iem.pub.ro/rrst-ee/article/view/111/168

[30] P. Kumar, M. Kumar, N. Pal, "An efficient control approach of voltage and frequency regulation in an autonomous microgrid", Revue Roumaine des Sciences Techniques - Serie Electrotechnique et Energetique, vol. 66, no. 1, 2021, pp. 33–39. [Online]. https://journal.iem.pub.ro/rrst-ee/article/view/63/47

[31] Ordin nr. 228/2018 pentru aprobarea Normei tehnice "Condiții tehnice de racordare la rețelele electrice de interes public pentru prosumatorii cu injecție de putere activă în rețea", emitent ANRE - Autoritatea Națională de Reglementare în Domeniul Energiei. [Online]. https://lege5.ro/gratuit/gmytimzvhe4a/ordinul-nr-228-2018-pentru-aprobarea-normei-tehnice-conditii-tehnice-de-racordare-la-retelele-electrice-de-interes-public-pentru-prosumatorii-cu-injectie-de-putere-activa-in-retea

[32] https://www.greenpeace.org/romania/articol/1198/lucian-popescu-primul-roman-care-s-a-conectat-la-retea-cu-un-sistem-fotovoltaic-pentru-a-obtine-energie-curata/

[33] Directive 2018/2001 of the european parliament and of the council on the promotion of the use of energy from renewable sources, Official Journal of the European Union, 2018. [Online]. https://eur-lex.europa.eu/legal-content/en/TXT/PDF/?uri=CELEX:32018L2001

[34] https://anre.ro/wp-content/uploads/2023/05/Raport-prosumatori_2022.pdf

[35] M. Shafiullah, S. D. Ahmed, F. A. Al-Sulaiman, "Grid Integration Challenges and Solution Strategies for Solar PV Systems: A Review", IEEE Access, vol. 10, 2022, pp. 52233-52257, [Online]. doi:10.1109/ACCESS.2022.3174555

[36] Commission Regulation (EU) 2019/1782 laying down ecodesign requirements for external power supplies pursuant to Directive 2009/125/EC of the European Parliament and of the Council and repealing Commission Regulation (EC) No 278/2009, Official Journal of the European Union, 2019. [Online]. Available: https://eur-lex.europa.eu/legal-content/EN/TXT/PDF/?uri=CELEX:32019R1782&from=es

[37] https://creator.fronius.com/pv-design

[38] International Standard ISO 2859-1, "Sampling procedures for inspection by attributes - Part 1: Sampling plans indexed by acceptable quality level (AQL) for lot-by-lot inspection", First edition, 1989, [Online]. https://sites.chemistry.unt.edu/~tgolden/courses/iso2859-1.pdf

[39] https://www.victronenergy.ro/panel-systems-remote-monitoring/vrm

[40] https://www.victronenergy.ro/upload/documents/Datasheet-MultiPlus-II-inverter-charger-RO.pdf

[41] United States Advanced Battery Consortium (USABC) - Battery Test Manual For Electric Vehicles, U. S. Department of Energy Vehicle Technologies Program, revision 3.1, 2020. [Online]. https://cet.inl.gov/ArticleDocuments/USABCElectricVehicleTestManualRev3.1.pdf

[42] E. Barsoukov, J. R. Macdonald, "Impedance Spectroscopy Theory, Experiment, and Applications", Second Edition, Chapter 3.3, Wiley-Interscience, 2005, pp. 188-204. [Online]. https://www.biodyn.ro/course/literatura/Impedance%20Spectroscopy%20Theory%20Experiment%20And%20Applications%20Wiley%202004.pdf

[43] M. Orazem, B. Tribollet, "Electrochemical Impedance Spectroscopy", ECSThe Electrochemical Society Series, Wiley-Interscience, 2008. [Online]. https://www.researchgate.net/profile/Mazdak_Izadi/post/From_where_can_I_learn_about_Nyquist_and_bode_plots/attachment/59d6595979197b80779aee46/AS:542110975619072@1506260736303/download/Orazem+EIS.pdf

[44] C. Pastor-Fernandez, K. Uddin, G. H. Chouchelamane, W. D. Widanage, J. Marco, "A Comparison between Electrochemical Impedance Spectroscopy and Incremental Capacity-Differential Voltage as Li-ion Diagnostic Techniques to Identify and Quantify the Effects of Degradation Modes within Battery Management Systems", Journal of Power Sources, vol. 360, 2017, pp. 301-318. [Online]. doi: 10.1016/j.jpowsour.2017.03.042

[45] Ordonanţă de urgenţă 27/2022 privind măsurile aplicabile clienţilor finali din piaţa de energie electrică şi gaze naturale în perioada 1 aprilie 2022-31 martie 2023, Articolul 1, litera B [Online]. https://lege5.ro/Gratuit/geydsnbsgi3dk/art-1-ordonanta-de-urgenta-27-2022?dp=gq2tmnrrgu2tiny